

2011

## ESTIMATION OF THE ORTHOTROPIC ELASTIC PROPERTIES OF THE RAT EARDRUM

Ehsan Salamati

Follow this and additional works at: <https://ir.lib.uwo.ca/digitizedtheses>

---

### Recommended Citation

Salamati, Ehsan, "ESTIMATION OF THE ORTHOTROPIC ELASTIC PROPERTIES OF THE RAT EARDRUM" (2011). *Digitized Theses*. 3346.  
<https://ir.lib.uwo.ca/digitizedtheses/3346>

This Thesis is brought to you for free and open access by the Digitized Special Collections at Scholarship@Western. It has been accepted for inclusion in Digitized Theses by an authorized administrator of Scholarship@Western. For more information, please contact [wlsadmin@uwo.ca](mailto:wlsadmin@uwo.ca).

THE UNIVERSITY OF WESTERN ONTARIO  
SCHOOL OF GRADUATE AND POSTDOCTORAL STUDIES  
**ESTIMATION OF THE ORTHOTROPIC ELASTIC PROPERTIES OF THE RAT  
EARDRUM**  
CAPTOR'S DEPT OF ENGINEERING

(Spine title: Orthotropic Elastic Properties of the Eardrum)

(Thesis format: Integrated-Article)

by

**Ehsan Salamati**

Graduate Program in Electrical and Computer Engineering

A thesis submitted in partial fulfillment  
of the requirements for the degree of  
Master of Engineering Science

School of Graduate and Postdoctoral Studies  
The University of Western Ontario  
London, Ontario, Canada

ESTIMATION OF THE ORTHOTROPIC ELASTIC PROPERTIES OF THE RAT  
EARDRUM  
© Ehsan Salamat 2011

THE UNIVERSITY OF WESTERN ONTARIO  
SCHOOL OF GRADUATE AND POSTDOCTORAL STUDIES

**CERTIFICATE OF EXAMINATION**

Joint-Supervisor

\_\_\_\_\_  
Dr. Hanif Ladak

Joint-Supervisor

\_\_\_\_\_  
Dr. Abbas Samani

Supervisory Committee

\_\_\_\_\_  
Dr. Sumit K. Agrawal

Examiners

\_\_\_\_\_  
Dr. James Lacefield

\_\_\_\_\_  
Dr. Shaun Salisbury

\_\_\_\_\_  
Dr. Daniel Goldman

The thesis by

**Ehsan Salamati**

entitled:

**ESTIMATION OF THE ORTHOTROPIC ELASTIC PROPERTIES OF THE RAT  
EARDRUM**

is accepted in partial fulfillment of the  
requirements for the degree of  
Master of Engineering Science

Date \_\_\_\_\_

\_\_\_\_\_  
Chair of the Thesis Examination Board

## Abstract

Finite-element (FE) models of the eardrum have been developed to understand its impedance-matching function. Modeling accuracy depends on the assumed elastic properties. Although the eardrum is an orthotropic elastic structure, for simplicity, most investigators have measured the eardrum's elastic properties while assuming it is isotropic. No data are available in the literature on the eardrum's orthotropic elastic properties. In this work, existing indentation-based and pressurization-based methods were extended for estimating the orthotropic elastic properties of the eardrum *in situ*. For the pressurization-based method, an accuracy in excess of 90% is achieved when the signal-to-noise ratio (SNR) is 2 or greater, while an SNR of 200 or greater is required for the indentation-based method. The indentation-based method was applied to the rat eardrum for which measurements were available, yielding average values of  $E_x = 23.39 \pm 1.55$  MPa,  $E_y = 58.67 \pm 4.16$  MPa, and  $G_{xy} = 35.56 \pm 3.29$  MPa.

**Keywords:** eardrum, orthotropic elastic properties, optimization, finite element modeling, indentation-based method, pressurization-based method.

## **Co-Authorship**

Chapter 2 of the thesis contains a manuscript prepared for submission to *The Journal of Medical and Biological Engineering* (JMBE) entitled “Estimation of the orthotropic elastic properties of the rat eardrum”. This chapter was co-authored by Ehsan Salamati, Dr. Sumit Agrawal, Dr. Abbas Samani and Dr. Hanif Ladak. Ehsan Salamati implemented, tested and applied the estimation algorithms and wrote an initial draft of the manuscript. Dr. Ladak and Dr. Samani were Ehsan Salamati’s program supervisors. They provided the objectives and directions for the project. Dr. Agrawal, an ear surgeon, assisted in specimen dissection and preparation.

## **Dedication**

I would like to dedicate my thesis with all my heart to my beloved family, to my father and mother, for dedicating their whole life in my upbringing and for instilling the value of patience in my life, and to my sister for her support of my academic endeavors.

## Acknowledgments

I would like to thank my supervisors Dr. Abbas Samani and Dr. Hanif Ladak for their guidance and insightful criticisms. I am grateful to Dr. Sumit Agrawal for his training related to specimen dissection and preparation. I would like to thank Seyyed Mohamad Hesabgar and Seyed Reza Mousavi for their technical support. Also, I would like to thank all of my colleagues during my studies who helped me pursue my work in a better way and for creating a friendly environment in the laboratory.

Funding for this work was provided by the Natural Sciences and Engineering Research Council of Canada and by the University of Western Ontario.

## Table of Contents

CERTIFICATE OF EXAMINATION .....	ii
Abstract .....	iii
Co-Authorship.....	iv
Dedication .....	v
Acknowledgments.....	vi
Chapter 1 .....	1
1.1. Introduction.....	1
1.1.1. Motivation.....	1
1.2. Structure and function of the ear.....	2
1.2.1. Gross anatomy and function of the human eardrum .....	5
1.2.2. Ultrastructure of the eardrum .....	7
1.2.3. Rat middle ear.....	9
1.3. Theory .....	10
1.3.1. Theory of elasticity.....	10
1.3.2. Finite Element Method .....	19
1.3.3. Inverse problem .....	20
1.4. Literature review .....	21
1.4.1. Previous eardrum mechanics works under the assumption of isotropy .....	21
1.4.2. Previous eardrum mechanics works under the assumption of orthotropy.....	26
1.5. Objective .....	26
1.6. References.....	28
Chapter 2.....	32
2.1. Introduction.....	32
2.2. Materials and Method .....	36
2.2.1. Overview .....	36
2.2.2. FE model construction .....	37
2.2.3. Generating Synthetic Data.....	43
2.2.4. Optimization .....	44
2.2.5. Experimental indentation data .....	47
2.3. Results.....	49



2.3.1 Algorithm testing on synthetic data .....	49
2.3.2. Estimate from actual indentation data .....	50
2.3.3. Variation of model parameters.....	52
2.4. Discussion .....	54
2.4.1. Algorithm testing on synthetic data .....	54
2.4.2. Application to actual indentation data .....	55
2.5. Conclusion .....	57
2.4. References.....	58
Chapter 3.....	62
3.1. Contributions.....	62
3.2. Future Considerations .....	63
3.2. Reference .....	66
CURRICULUM VITAE.....	68

## List of Figures

Figure 1.1: The human ear .....	3
Figure 1.2: The human eardrum .....	4
Figure 1.3: Schematic of the interior of right inner ear .....	5
Figure 1.4: Outline of the human eardrum .....	6
Figure 1.5: The ultrastructure of the eardrum .....	8
Figure 1.6: The fiber arrangement of the pars tensa .....	8
Figure 1.7: Comparison between rat and human eardrum .....	10
Figure 1.8: Two components of stress at a point within a deformable body .....	11
Figure 1.9: Stress tensor in a loaded deformable continuum material body .....	13
Figure 1.10: A typical stress-strain relationship of soft tissues .....	15
Figure 1.11: Three basis vectors of orthotropic material .....	18
Figure 1.12: 3D FEM mesh .....	20
Figure 2.1: The estimation flowchart .....	36
Figure 2.2: Illustration of basic TFI meshing algorithm .....	39
Figure 2.3: Three basic steps for generating an FE mesh of the eardrum .....	40
Figure 2.4: A typical FE mesh for a rat eardrum .....	42
Figure 2.5: Ground truth and recovered values of in-plane shear modulus for the indentation-based method .....	49
Figure 2.6: Ground truth and recovered values of in-plane shear modulus for the pressurization -based method .....	50
Figure 2.7: Experimental and corresponding simulated force-displacement curve .....	51
Figure 2.8: variation in optimal orthotropic parameters of the pars tensa .....	53

## List of Tables

Table 1: Initial guess sets .....	47
Table 2: Estimated orthotropic parameters for each sample pars tensa .....	50

# Chapter 1

## 1.1. Introduction

### 1.1.1. Motivation

Computer models have become a standard tool across many aspects of hearing research, especially in understanding the acoustics and mechanics of the auditory system. In particular, the finite-element (FE) method has gained popularity because of its ability to handle complex shapes, material properties and loading and boundary conditions with relative ease. As the eardrum plays a major role in hearing, understanding its function is of great importance. FE models of the eardrum can potentially provide insight into the function of the eardrum and could be used to improve diagnostic and surgical procedures (Funnell and Laszlo, 1978). One potential application of an FE model of the eardrum is in tympanometry, a diagnostic procedure which is used to test the mobility of the eardrum and middle-ear bones by applying a sequence of large static pressures in the ear canal. An FE model could be used to extract more diagnostic information from tympanometry and could lead to improved pathology diagnosis (Daniel *et al*, 2001). For instance, it could help clinicians understand confounding factors such as the contributions of the pliable ear canal of newborns to tympanometric measurements.

Apart from improving diagnostic procedures, eardrum modeling could also be useful in optimizing surgical procedures. For instance, myringotomy is a procedure in which a small incision is made in the eardrum and a ventilation tube is inserted to alleviate middle-ear infection. Designing an optimal shape for a ventilation tube and determining

the best insertion location using an FE model can lead to improved post-surgical hearing outcomes (Ferris and Prendergast, 1999).

Another application of models is in myringoplasty which involves repairing holes in the eardrum using grafts. The mechanical properties of the graft material and its size are very important determinants of the mechanical function of the repaired eardrum (Zahnert *et al*, 2000). An FE model can be employed to find suitable materials and shapes before fabricating actual grafts and undertaking costly clinical trials (Lee *et al*, 2006; Lee *et al*, 2007).

In order to benefit from FE models of the eardrum in the above-mentioned applications, the mechanical properties of eardrum are required as input to these models. The accuracy of FE models is significantly dependent on the mechanical properties used as input (Funnell and Laszlo, 1978). As would be expected, the mechanical properties of the eardrum are dependent on its structure which is described in the next section. Section 1.3 provides some theoretical background on the theory of elasticity, on the FE method and on inverse problems to put the literature review in Section 1.4 concerning the eardrum mechanical properties into context.

## **1.2. Structure and function of the ear**

The auditory system is subdivided into three major parts: the external ear, the middle ear and the inner ear which are shown in Figure 1.1. This study is focused on the middle ear, especially the eardrum, hence only the anatomy and function of the middle ear and eardrum are covered in depth. The external ear consists of the auricle and ear canal. The auricle is the visible part of the ear that collects sound waves and directs them to the

external auditory canal (ear canal). The middle ear includes several air-filled cavities which are separated from the ear canal by the eardrum. The eardrum separates the middle ear from the ear canal, and vibrates in response to sound waves in the ear canal. Mechanical vibrations of the eardrum are transferred across the middle-ear cavities by the ossicles to the inner ear. As shown in Figure 1.2, the ossicles (i.e., bones) link the eardrum to the inner ear and consist of the malleus, the incus, and the stapes. The long process of the malleus is called the manubrium and is coupled to the medial side of the eardrum, and the head of the malleus is connected to the incus. The other end of the incus is connected to the stapes. The footplate of the stapes is located on the oval window of the cochlea, which is part of the inner ear. The ossicles are suspended in the cavities by ligaments and are acted upon by two muscles: the tensor tympani which is attached to the malleus and the stapedius muscle which connects to the stapes.

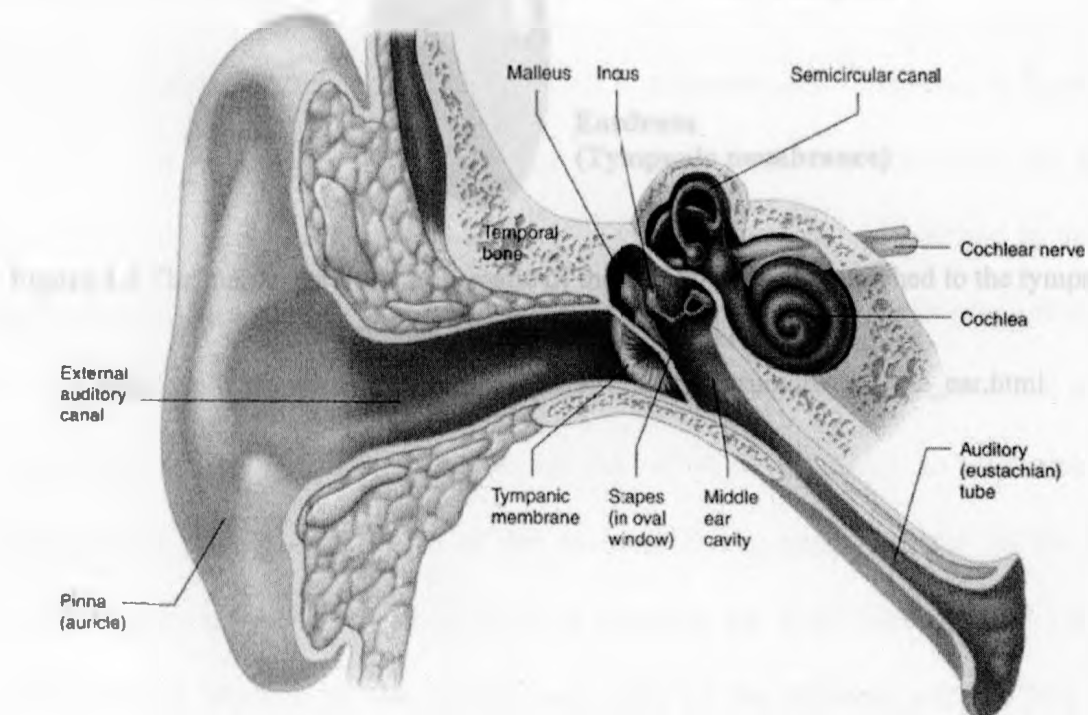


**Figure 1.1** The human ear. Anatomy of the human ear. From Vander *et al*, (2004).

The inner ear, which is shown in detail in Figure 1.3, is located medial to the middle ear, and consists of the cochlea, vestibule and semicircular canals. Only the cochlea is related to hearing, whereas the vestibule and semicircular canals are organs of balance. The oval window is a membrane underneath the footplate of the stapes. Through this window, vibrations of the stapes are transferred to the liquid inside the cochlea. Motion of the cochlear fluid causes movement of hair cells inside the cochlea. These hair cells are responsible for transduction of fluid motion to nerve impulses that are transferred to the brain for further processing.

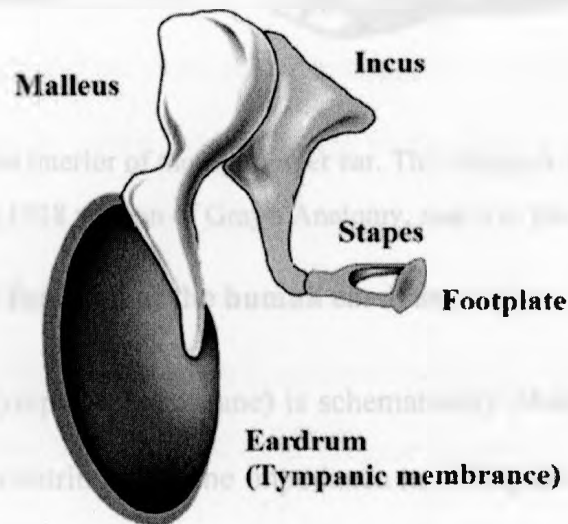


**Figure 1.2** The human eardrum. Schematic of the auditory ossicles attached to the tympanic membrane. This image is a reproduction of

[http://www.psywww.com/intropsych/ch04\\_senses/structures\\_of\\_the\\_ear.html](http://www.psywww.com/intropsych/ch04_senses/structures_of_the_ear.html)

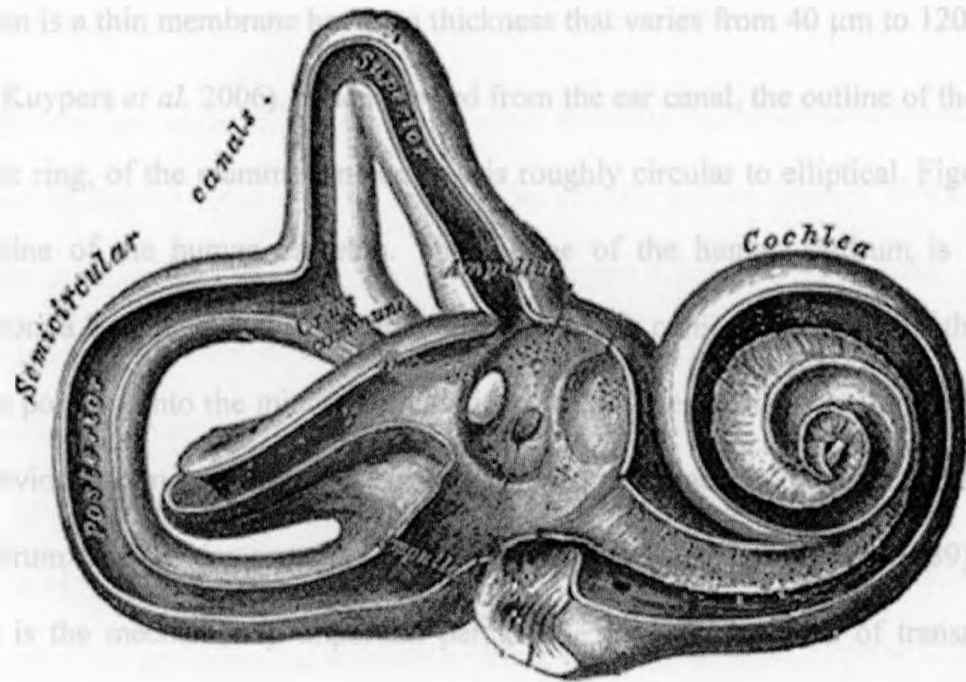


**Figure 1.3** Schematic of the interior of the right inner ear. This image is a reproduction of a lithograph plate from a 1918 version of Gray's Anatomy, and is in the public domain.

### 1.2.1. Gross anatomy and function of the human eardrum

The eardrum (also called tympanic membrane) is schematically illustrated in Figure 1.4. The eardrum is the major contributor to the impedance matching function of the middle ear in which the low acoustic impedance of air in the ear canal is matched to the high acoustic impedance of the cochlear fluids. Here, impedance is defined as pressure divided by volume velocity, and is an indicator of the resistance to the flow of acoustical energy. If sound is directly transferred from air (as in the ear canal) to sea water (an approximation of the composition of the cochlear fluid), approximately 99.9% of the acoustic energy reflects back to air without entering the fluid (Durrant and Lovrinic, 1977). Thus in absence of the middle ear, most of the acoustic energy fails to be transferred from the ear canal to the cochlea.



The eardrum is a thin membrane having a thickness that varies from 40  $\mu\text{m}$  to 120  $\mu\text{m}$  at its center (Kuypers *et al*, 2006). When viewed from the ear canal, the outline of the base, or tympanic ring, of the mammalian eardrum is roughly circular to elliptical. Figure 1.4 shows outline of the human eardrum. The outline of the human eardrum is almost circular. From a 3-dimensional perspective, the eardrum is conical in shape with the apex of the cone pointing into the middle-ear cavities and the sides of the cone formed by the eardrum having varying curvature. The pars tensa and pars flaccida comprise the surface of the eardrum and are demarcated in Figure 1.4 (Dirckx and Decraemer, 1989). The pars tensa is the mechanically important part of the eardrum in terms of transmitting vibrations caused by sound in the ear canal to the middle-ear ossicles. The manubrium is a process of the malleus that is tightly coupled to the medial side of the pars tensa. The most inferior point of the manubrium is called the umbo which forms the apex of the cone formed by the eardrum. The pars flaccida is a smaller portion of eardrum located superior to the pars tensa. This part is more compliant compared to the pars tensa. The pars flaccida is separated from the pars tensa by an annular ligament.

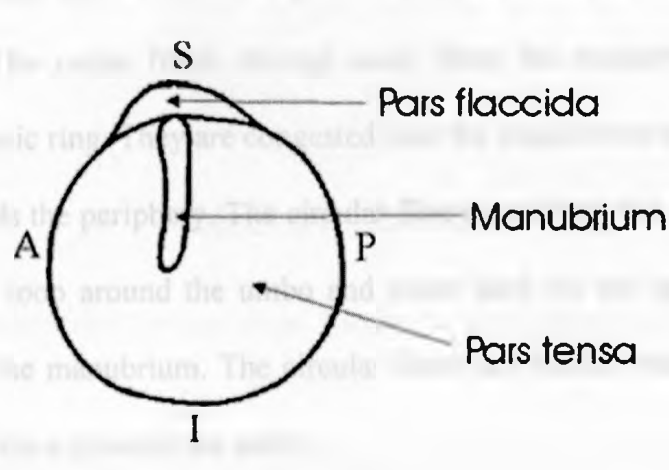


**Figure 1.4** Outline of the human eardrum as viewed from the ear canal. A: anterior, I: inferior, P: posterior, S: superior. This figure is reproduction of a figure in Funnell (1975).

### 1.2.2. Ultrastructure of the eardrum

The eardrum can be described as a multi-layer structure that consists of three layers: (1) an outer epidermal layer on the lateral side, (2) the lamina propria which is the intermediate layer, and (3) an inner mucosal layer. Figure 1.5 shows a schematic view of the ultrastructure of the human pars tensa (Lim, 1995). The epidermal layer is continuous with the epidermal lining of the ear canal. It is epithelium with no glands or hair follicles. The inner mucosal layer is continuous with the mucosal lining of the middle ear. It consists of a very thin layer of cells. The lamina propria, as shown in Figure 1.5, consists of four layers: (1) a subepidermal connective tissue layer, (2) an inner circular fiber layer, (3) an outer radial fiber layer, and (4) a submucosal connective tissue layer. The subepidermal and submucosal layers are similar and consist of loose connective tissue. Both layers have vascular plexus and nerve network.

The radial and circular fiber layers are the mechanically important structures of the pars tensa and thus of the eardrum. As shown in Figure 1.6, they are highly organized fiber layers where each layer contains a parallel set of fibers held in small volume of ground substance. The radial fibers diverge away from the manubrium more or less straight to the tympanic ring. They are congested near the manubrium and spread out with lower density towards the periphery. The circular fibers start from the superior portion of the manubrium and loop around the umbo and insert back on the opposite side of the superior portion of the manubrium. The circular fibers are thicker near the periphery of the pars tensa and reduce towards the umbo.

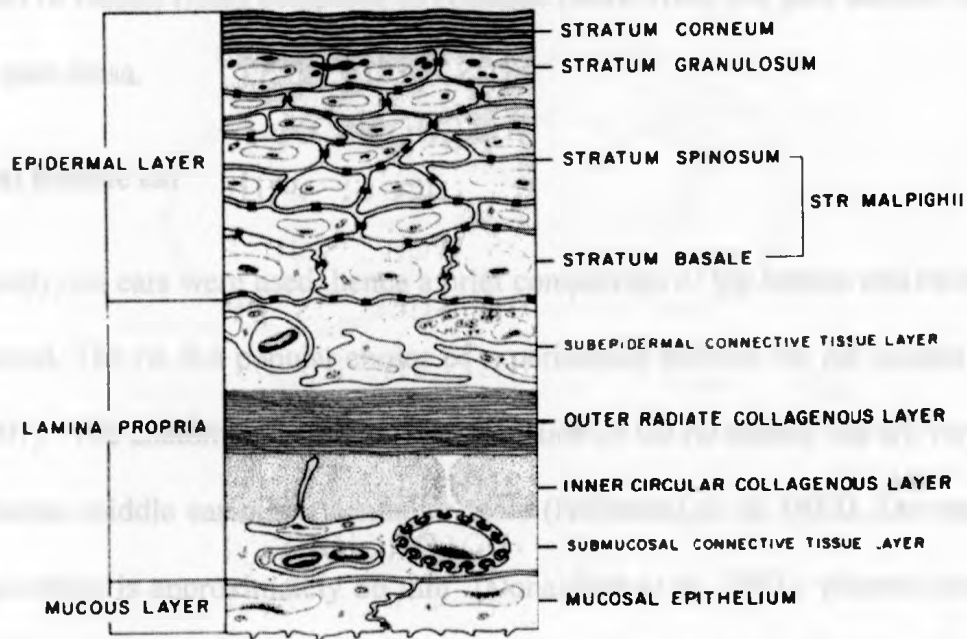


**Figure 1.5** The ultrastructure of the eardrum. Cross-section through the pars tensa of the human eardrum with the epidermal layer, lamina propria , and the mucous layers. This figure is reproduction of a figure in Lim (1995).

### Circular fibers



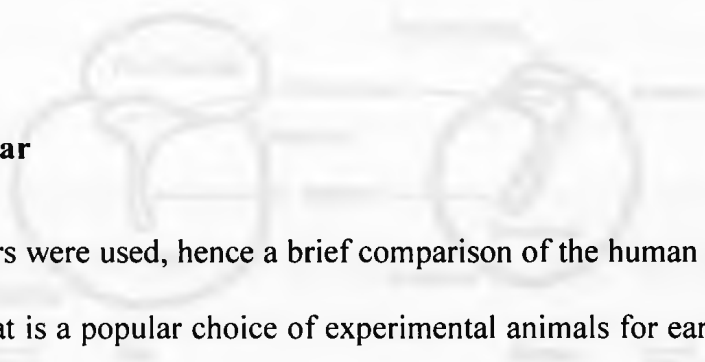
### Radial fibers

**Figure 1.6** Fiber arrangement of the pars tensa. This figure is reproduction of a figure in Luo *et al*, (2009).

The ultrastructure of the pars flaccida is similar to that of the pars tensa except that the lamina propria of the pars flaccida does not have the highly organized fibrous layers found in the lamina propria of the pars tensa, and the pars flaccida contains a higher

proportion of elastin fibers compared to collagen fibers. Also, the pars flaccida is thicker than the pars tensa.

### 1.2.3. Rat middle ear



In this study, rat ears were used, hence a brief comparison of the human and rat eardrums is warranted. The rat is a popular choice of experimental animals for ear studies (Akache *et al*, 2007). The anatomical structures and function of the rat middle ear are very similar to the human middle ear but at a smaller scale (Hellstrom *et al*, 1982). The area of the human eardrum is approximately 66 mm<sup>2</sup> (Donaldson *et al*, 1992), whereas the area of the rat eardrum is approximately 11 mm<sup>2</sup> (Zimmer *et al*, 1994). Another difference between the human and rat eardrums is the relative size of the pars tensa to the pars flaccida. The human eardrum has a very small pars flaccida relative to the total size of the eardrum. However, the pars flaccida occupies between one-third to one-quarter of the total area of the rat eardrum. A visual comparison of the human and rat eardrums is shown in Figure 1.7.

The short process of malleus in rat points towards posterior wall while it points towards anterior wall in humans. Furthermore, rat malleus is slightly curved towards the lower wall; however, it leans towards the posterior wall in human (Castagno *et al*, 2006).

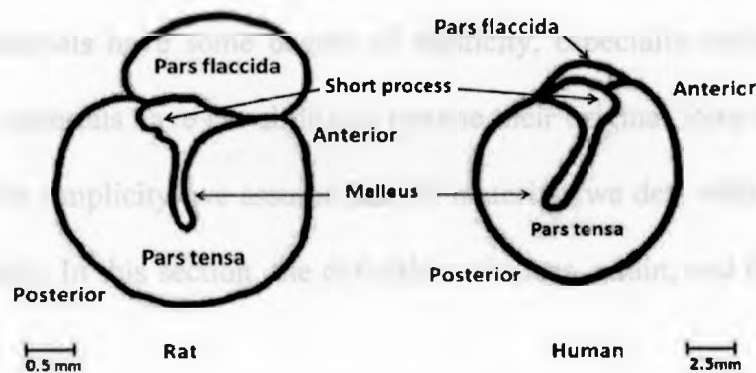


**Figure 1.7** Comparison between rat and human eardrum. This figure is reproduction of a figure in Castagno *et al*, (2006).

### 1.3. Theory

#### 1.3.1. Theory of elasticity

All materials consist of molecules which are their distinct building blocks. Thus, they are inherently discontinuous. However, we can assume that solid materials are a continuum as long as the problem of interest is being investigated at a length much larger than the material's inter-atomic distance. With this condition, the continuum material idealization is highly accurate. Under continuum assumption, the substance of the body fills the entire space that the object occupies completely. Therefore, any point within the body is assumed to contain material. Continuum mechanics is a branch of science that tackles the mechanical behavior of continuum materials. This includes deformation and fracture of such material under loading. All materials deform when subjected to forces. The theory of elasticity is a branch of continuum mechanics that considers the continuum material as elastic. Elastic materials are materials that lose their deformation and regain their original shape after forces applied to them are removed. Elasticity is the property that describes

the mechanical behavior of such materials, and the materials are called elastic materials. All structural materials have some degree of elasticity, especially under small strains. Perfectly elastic materials have the ability to resume their original form completely after force removal. For simplicity, we assume that all materials we deal with in this research are perfectly elastic. In this section, the definition of stress, strain, and their relationship are presented.

### 1.3.1.1. Stress

Stress is a measure of force per unit area within an object as a result of applying external forces. Stress has the same unit as pressure and is measured in force per area units such as  $\left(\frac{\text{Newton}}{\text{m}^2}\right)$  or *Pascal*. The stress can be decomposed into two components depending on the force and its relative orientation of the plane under consideration. As shown in Figure 1.8, these two components are the normal stress ( $\sigma$ ), which arises from perpendicular force component to the cross-sectional area of the material, and shear stress ( $\tau$ ), which arises from the force component lying within the plane of the cross-sectional area.

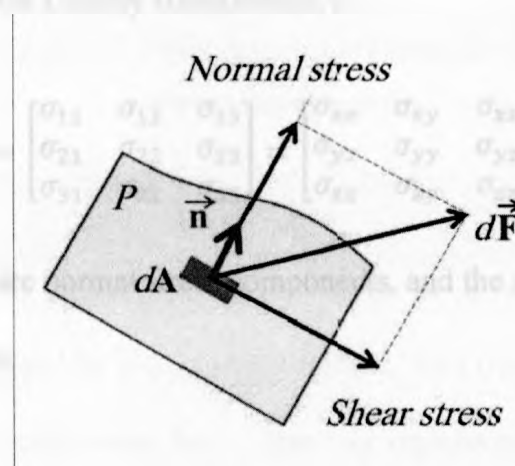


**Figure 1.8** Two components of stress at a point within a deformable body

Mathematically, the stress is defined as the limit of the force distributed over an area when the area tends to zero:

$$\sigma = \lim_{dA \rightarrow 0} \frac{dF_n}{dA} \quad (1-1)$$

$$\tau = \lim_{dA \rightarrow 0} \frac{dF_s}{dA} \quad (1-2)$$

where  $dF_n$  and  $dF_s$  are the normal and tangential components of the force  $dF$  acting on an infinitesimal area  $dA$  at point  $P$ .

The stress involves two vectors of force and surface. In 3D, at any given point  $P$ , depending on the orientation of the plane passing through it, in general there will be one normal and two shear stress components. Including that plane, one can imagine that a very small cubic element can be formed around point  $P$ . This cube has 6 faces where each face has one normal and two shear stress components as shown in Figure 1.9. As such, the stress is a tensor quantity, and according to Cauchy (A. Mohammed, 2005), the stress is assumed to be continuum at any point within the material, and is defined by second-order tensor, known as the Cauchy stress tensor,  $\sigma$ :

$$\sigma = \begin{bmatrix} \sigma_{11} & \sigma_{12} & \sigma_{13} \\ \sigma_{21} & \sigma_{22} & \sigma_{23} \\ \sigma_{31} & \sigma_{32} & \sigma_{33} \end{bmatrix} = \begin{bmatrix} \sigma_{xx} & \sigma_{xy} & \sigma_{xz} \\ \sigma_{yx} & \sigma_{yy} & \sigma_{yz} \\ \sigma_{zx} & \sigma_{zy} & \sigma_{zz} \end{bmatrix} \quad (1-3)$$

where  $\sigma_{11}$ ,  $\sigma_{22}$ , and  $\sigma_{33}$  are normal stress components, and the six other parameters are the shear stress components.

If a body is in static equilibrium, the Cauchy stress tensor at any point within the body satisfies the equilibrium equations:

$$\sigma_{ji,j} + F_i = 0 \quad (1-4)$$

where the  $\sigma$  indices follow Einstein's convention and  $F_i$  represents body forces. Also, equilibrium requires that the summation of moments with respect to an arbitrary point equals zero. This leads to the conclusion that the stress tensor is symmetric:

$$\sigma_{ij} = \sigma_{ji} \quad (1-5)$$

Therefore,  $\sigma_{12} = \sigma_{21}$ ,  $\sigma_{13} = \sigma_{31}$ ,  $\sigma_{32} = \sigma_{23}$ , and the Cauchy stress tensor has only six independent parameters.

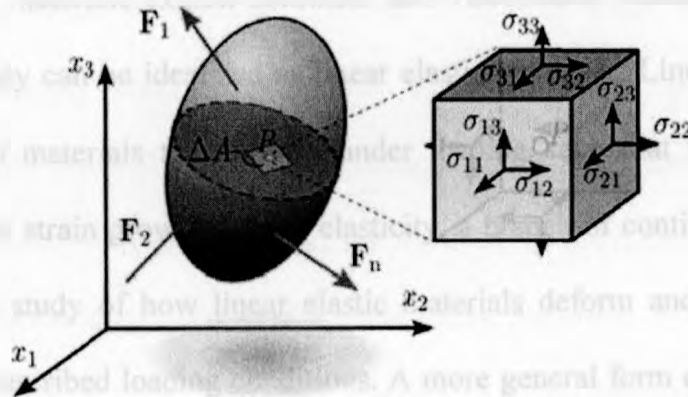


**Figure 1.9** Stress tensor in a loaded deformable continuum material body (Source: [www.wikipedia.com](http://www.wikipedia.com)).

### 1.3.1.2. Strain

Strain is a normalized measure of deformation of a continuum body. Material deformation is characterized by a displacement field. This field is defined as a change in the configuration of a continuum body from an undeformed to a current deformed configuration. Like stress, strain has two types, normal and shear. Normal strain is defined as relative displacement of a point within a body per unit length along a particular



direction. Shear strain is defined as relative rotation of each two perpendicular planes in the body. Again, similar to stress, strain is a tensor quantity and is represented by a matrix with 6 independent components as follows.

$$\varepsilon = \begin{bmatrix} \varepsilon_{11} & \varepsilon_{12} & \varepsilon_{13} \\ \varepsilon_{21} & \varepsilon_{22} & \varepsilon_{23} \\ \varepsilon_{31} & \varepsilon_{32} & \varepsilon_{33} \end{bmatrix} = \begin{bmatrix} \varepsilon_{xx} & \varepsilon_{xy} & \varepsilon_{xz} \\ \varepsilon_{yx} & \varepsilon_{yy} & \varepsilon_{yz} \\ \varepsilon_{zx} & \varepsilon_{zy} & \varepsilon_{zz} \end{bmatrix} \quad (1-6)$$

where  $\varepsilon_{11}$ ,  $\varepsilon_{22}$ , and  $\varepsilon_{33}$  are normal strain components, and the six other parameters are the shear strain components. The strain is dimensionless.

### 1.3.1.3. Linear elasticity

While in general, materials exhibit nonlinear and viscoelastic mechanical behavior, for many purposes they can be idealized as linear elastic materials. Linear elastic materials are a category of materials that deform under loading such that the stress increases proportional to the strain growth. Linear elasticity, a branch of continuum mechanics, is the mathematical study of how linear elastic materials deform and become internally stressed due to prescribed loading conditions. A more general form of this mathematical study is the nonlinear theory of elasticity where the stress grows in a nonlinear fashion with strain growth. In linear elasticity, there is a linear relationship between strain tensor components and derivatives of displacement components. Also, stress and strain tensors have a linear relationship. A typical stress-strain relationship for soft tissue material is depicted in Figure 1.10.

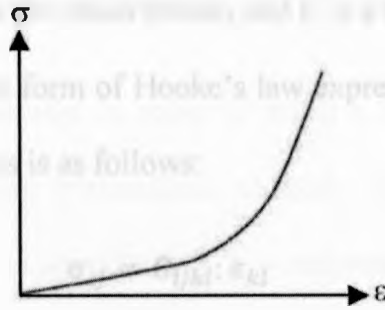


**Figure 1.10** A typical stress-strain relationship of soft tissues.

In this figure, a linear behavior is observed up to a certain point beyond which the mechanical behavior becomes nonlinear.

The fundamental linear elasticity assumptions are: small deformation which leads to small strains, and linear relationship between stress and strain components. Linear elasticity is commonly used in structural analysis because the abovementioned assumptions are reasonable for many engineering materials. In general, the stress-strain relationship of a material is referred to as the material's constitutive equation. Hooke's law is the general constitutive equation for linear elastic materials.

#### 1.3.1.4. Hooke's law

The relation which describes the stress developed in a deformed body was first identified by Robert Hooke. This relation is linear between stress and strain components, which is a reasonable approximation for many elastic materials. Hooke's law in its general form is as follows:

$$\sigma = C: \epsilon \quad (1-7)$$

Where  $\sigma$  is the stress tensor,  $\epsilon$  is the strain tensor, and  $C$  is a fourth-order tensor called the stiffness tensor. The generalized form of Hooke's law expressed in terms of components with respect to orthonormal basis is as follows:

$$\sigma_{ij} = C_{ijkl} \epsilon_{kl} \quad (1-8)$$

The stiffness tensor as a fourth-order tensor contains 81 elastic constants. However, it can be demonstrated that the number of independent constants is reduced to only 21 elastic constants due to the symmetry of stress, and strain tensors. In other words

$$[C_{ij}] = \begin{bmatrix} C_{11} & C_{12} & C_{13} & C_{14} & C_{15} & C_{16} \\ C_{12} & C_{22} & C_{23} & C_{24} & C_{25} & C_{26} \\ C_{13} & C_{23} & C_{33} & C_{34} & C_{35} & C_{36} \\ C_{14} & C_{24} & C_{34} & C_{44} & C_{45} & C_{46} \\ C_{15} & C_{25} & C_{35} & C_{45} & C_{55} & C_{56} \\ C_{16} & C_{26} & C_{36} & C_{46} & C_{56} & C_{66} \end{bmatrix} \quad (1-9)$$

### 1.3.1.5. Young's modulus

Material mechanical properties are usually measured using uniaxial test where a cylindrical material sample is loaded such that the stress and strain are one dimensional along the cylinder axis. In a solid material, the slope of the stress-strain curve obtained from a uniaxial test is called the tangent elastic modulus. In the linear portion of the curve, the relation between stress and strain is characterized by a constant linear tangent modulus called the Young's modulus. The Young's modulus is a measure of stiffness of a linear elastic material. It is defined as the ratio of uniaxial stress over the uniaxial strain in the range of stress in which Hooke's law holds. The Young's modulus has units of pressure since it is the ratio of the stress, which has units of pressure, over the strain, which is dimensionless.

### 1.3.1.6. Materials properties characterization

When studying materials, especially in order to select a material versus others for a structural design and engineering applications, a metric value to compare materials is needed. A material's property is described by a parameter that is used as a metric to quantify the property. A material property could be a function of independent variables or a constant value. Material properties can be different in different directions. Such materials are called anisotropic materials. As mentioned above, the stiffness matrix for fully anisotropic materials consists of 21 independent constants. However, the number of constants can be considerably reduced depending on the internal directional symmetry displayed by the material.

### 1.3.1.7. Isotropic materials

Isotropic materials exhibit identical mechanical properties in all directions. These materials are characterized by material properties which are independent of directions. As such, constitutive equations that represent isotropic materials are independent of coordinate systems. For isotropic material, Hooke's law can be expressed by only the two parameters of Young's modulus and Poisson's ratio:

$$\boldsymbol{\varepsilon} = \frac{1}{E} \boldsymbol{\sigma} - \frac{\nu}{E} [\text{tr}(\boldsymbol{\sigma})\mathbf{I} - \boldsymbol{\sigma}] \quad (1-10)$$

In this equation, the strain tensor is presented in terms of the stress tensor in matrix form.  $E$  is Young's modulus,  $\nu$  is Poisson's ratio,  $\boldsymbol{\varepsilon}$  is the strain tensor, and  $\boldsymbol{\sigma}$  is the stress tensor. Poisson's ratio is the ratio of transverse strain measured in the direction perpendicular to the applied force, over axial strain measured in the direction of the

applied force. This parameter characterizes the material's compressibility and it ranges from 0 for foam materials to 0.5 for fully incompressible materials.

### 1.3.1.8. Orthotropic materials

Orthotropic materials are a type of anisotropic materials. Such materials have three orthogonal planes of symmetry where the material properties are different along their normal vectors. Wood is an example of orthotropic material where its properties are different in the wood's axial, radial, and circumferential directions as illustrated in Figure 1.11.

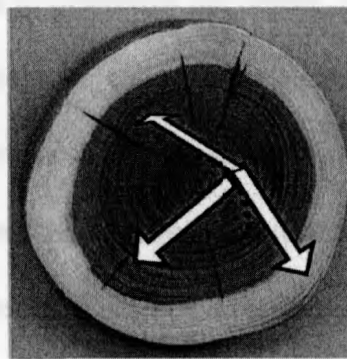


**Figure 1.11** Three basis vectors of orthotropic material. Three perpendicular basis vectors showing wood's orthotropic axial, radial, and circumferential symmetry directions.

For orthotropic materials, Hooke's law is expressed using the following equation:

$$\begin{bmatrix} \sigma_1 \\ \sigma_2 \\ \sigma_3 \\ \sigma_4 \\ \sigma_5 \\ \sigma_6 \end{bmatrix} = \begin{bmatrix} C_{11} & C_{12} & C_{13} & 0 & 0 & 0 \\ C_{21} & C_{22} & C_{23} & 0 & 0 & 0 \\ C_{31} & C_{32} & C_{33} & 0 & 0 & 0 \\ 0 & 0 & 0 & C_{44} & 0 & 0 \\ 0 & 0 & 0 & 0 & C_{55} & 0 \\ 0 & 0 & 0 & 0 & 0 & C_{66} \end{bmatrix} \begin{bmatrix} \epsilon_1 \\ \epsilon_2 \\ \epsilon_3 \\ \epsilon_4 \\ \epsilon_5 \\ \epsilon_6 \end{bmatrix} \quad (1-11)$$

As given in equation (1-11), for orthotropic materials the number of constants is reduced to 9 independent components. For thin orthotropic materials, the number of independent

components is reduced to only four constants. With such materials, only the four independent in-plane elastic constants are required to be determined. These constants are called the longitudinal and transverse Young's modulus ( $E_1$  and  $E_2$ ), in-plane shear modulus ( $G_{12}$ ), and the major Poisson's ratio ( $\nu_{12}$ ).

### 1.3.2. Finite Element Method

Many physical phenomena can be described by Partial Differential Equations (PDEs). In general, solving PDEs by classical analytical methods is almost impossible. The Finite-Element Method (FEM) is a numerical technique for finding approximate solutions of PDEs. The main idea of FEM is to discretize the object of interest's domain into a finite number of simple discrete subregions called finite elements. The resulting discretized domain is called a finite element mesh. Each element in the mesh has points, which are called finite element nodes, where the function of interest (e.g., displacement) is defined. Figure 1.12 illustrates a finite element mesh of a rectangular cuboid object. After domain discretization, the governing PDE is approximated into an algebraic equation which is valid for each finite element. Next, equations obtained for each element are assembled into a large system of equations that can be solved after applying the objects' boundary conditions. In structural analysis, the FEM is commonly used to solve static and dynamic problems.

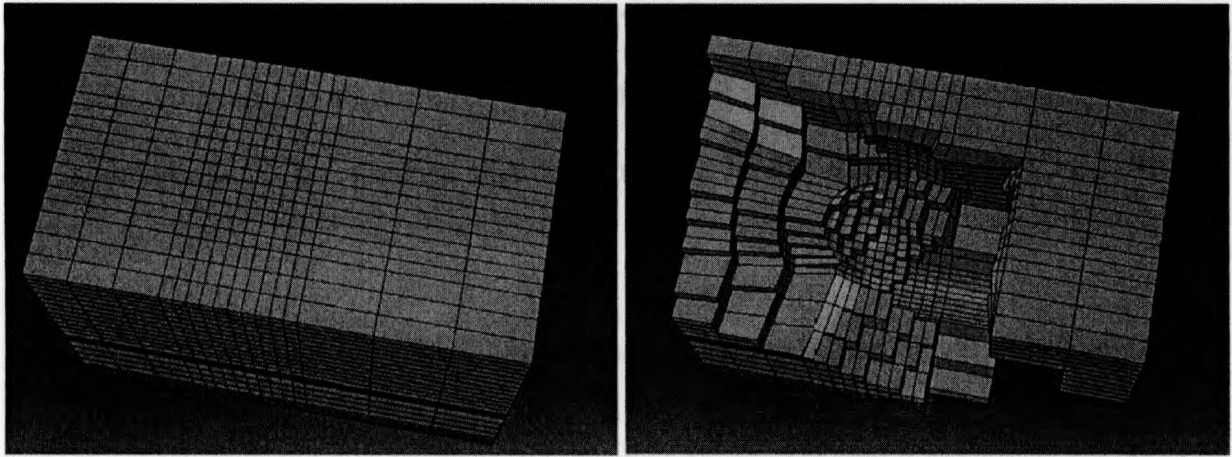


**Figure 1.12** 3D FEM mesh. Three dimensional FEM mesh of a solid rectangular cuboid object.

Various finite element types with different shapes can be used to discretize objects' domains. The complexity of the algebraic element equations approximating the governing PDE depends strongly on the element type. Mesh density and element type are the main factors that determine the problem's computational complexity and time required to obtain the solution.

Over the past decades FEM has been applied to simulate the mechanical behavior of the eardrum and to analyze its linear and nonlinear structural behavior as it has the capability of accurately dealing with complicated geometry and boundary conditions with relative ease. In this work, we have employed ABAQUS FE software package (Simulia Inc., RI, USA) to simulate the eardrum.

### **1.3.3. Inverse problem**

There are two general formulation frameworks to deal with problems encountered in science and engineering. These frameworks are known as forward problems and inverse problems. In forward problems, model parameters of a system are known and input stimulus is used to predict the system's output response. In other words, solution of a

forward problem involves determining the resulting output of a system given known input that describes the cause. In inverse problems, measured system response data (e.g., tissue deformation) are used as input to find the model parameters (e.g., the tissue orthotropic constants).

Inverse problems can be solved directly or iteratively. Often, inverse problems are formulated as optimization problems that are solved iteratively. In this case the corresponding forward problem is usually solved in each iteration.

#### **1.4. Literature review**

FE modeling is a powerful numerical method to investigate the function of the middle ear, (Elkhouri *et al*, 2006; Eiber, 1999; Sun *et al*, 2002; Koike *et al*, 2002), the effects of middle ear pathologies, (Gan *et al*, 2006), and the behavior of middle-ear prosthesis (Eiber *et al*, 2006).

##### **1.4.1. Previous eardrum mechanics works under the assumption of isotropy**

Although the fibrous ultrastructure of the pars tensa suggests it is not mechanically isotropic (exhibiting the same mechanical properties in all directions), the eardrum has been modeled with some success as an isotropic structure (Elkhouri *et al*, 2006). However, as noted by Fay *et al*, (2006), such models can only match the mechanical behavior of the eardrum over a limited range of frequencies. As mentioned before, linearly elastic isotropic tissues that are homogeneous can be characterized by a single Young's modulus value. The specific value of the Young's modulus has significant effect on the resulting response of FE models (Funnell *et al*, 1987; Elkhouri *et al*, 2006). Funnell (1987) reported that maximal displacement of the cat eardrum was reduced by



48% when Young's modulus of pars tensa was doubled in an FE model. However, maximal displacement increased by 79% when the Young's modulus was halved.

Uniaxial and beam-bending tests are the most common previous tests used to measure the Young's modulus of the eardrum. In a uniaxial test, a strip is cut out of the tissue and is gripped from one end, while the other end is subjected to a known tensile force parallel to the longitudinal axis of the sample. Then, the Young's modulus of the sample is defined as the ratio of stress over total strain. In a beam-bending test, again one end of a tissue strip is gripped and a force is applied to the other end perpendicular to the tissue strip's surface. The strip's deflection is measured instead of length change. The Young's modulus can then be estimated using a beam-bending formula. Although these two methods are commonly used, they have some critical flaws which affect the accuracy of the estimates.

Beam-bending and uniaxial tests both involve cutting tissues to prepare strip shape samples. As mentioned before, mechanical properties of the eardrum are mainly because of collagen fibers. Thus, cutting eardrum into strips compromises the structural integrity of the eardrum. Furthermore, non-uniform distribution of stress and strain within strips caused by cutting the eardrum into strip samples with geometrical irregularity is another source of error. Non-uniformity has a significant effect in measuring the Young's modulus of the eardrum since the tissue strips are short. The length of samples is dictated by the eardrum's size.

In the following review, the basic methods for measuring Young's modulus and their limitation are discussed. These shortcomings are the motivation for developing new

techniques to measure the mechanical properties of the eardrum under more accurate material assumptions.

Von Békésy (1960) estimated the Young's modulus of the eardrum for the first time. He performed a beam-bending test and reported a value of 20 MPa. His technique involved cutting the eardrum into a beam shape which compromises the structural integrity of the eardrum. Von Békésy's assumed that the pars tensa is homogeneous, so the Young's modulus value he reported is an "effective" one. Kirikae (1960) performed uniaxial tensile tests on small strips of the human eardrum, and he reported a value of 40 MPa. Unlike von Békésy who applied a static force in his experiments, Kirikae used a dynamic stimulus that involved oscillating eardrum strips at 890 Hz. Decraemer *et al*, (1980) performed similar uniaxial tensile tests on human cadaver eardrums, and they reported a value of 23 MPa. They also used dynamic stimuli, but in contrast to Kirikae, their experiments were done at 300 Hz. Again, these two works were done under the assumption of homogeneity in eardrum mechanical properties. Recently, Cheng *et al*, (2007) performed tensile tests on strips cut from human eardrums. They assumed that the eardrum is isotropic and homogeneous. They acquired stress-strain curves from uniaxial tests which were in good agreement with that of Decraemer *et al*, (1980). They reported that the Young's modulus value varies with stress from 0.4 MPa to 22 MPa as the stress varies from 0 to 1 MPa.

Huang *et al*, (2008) performed nanoindentation tests on the human eardrum after cutting the eardrum into small portions. They reported values of 19 MPa and 6 MPa for in-plane and through-thickness Young's modulus, respectively. Dhaphalapurkar *et al*, (2009) extended Huang's work by performing nanoindentation tests on small portions of fresh-

frozen human cadaveric eardrums. They measured values for the in-plane and through-thickness Young's modulus of relaxation. They noticed that the steady-state value of the Young's modulus varies among different samples. The steady-state values were in the range of 25.7 MPa to 37.8 MPa. Note that the nanoindentation test compromised the structural integrity of the eardrum because of cutting and leads to an estimate of local Young's modulus at the point subjected to indentation.

The eardrum is very fragile, has a complex geometry, and the human eardrum is small with major diameter of about 9 to 10 mm and minor diameter of 8 to 9 mm (Decraemer et al, 1991), and a minimum thickness on the order of 30  $\mu\text{m}$  (Kupers *et al*, 2006). Conducting uniaxial tensile tests, beam bending tests, and nanoindentation tests as described above after cutting out strips can be difficult and problematic.

Some of these issues were addressed by Gaihede *et al*, (2007) using a hydraulic system in order to apply pressure to the intact eardrum (i.e., the eardrum was not cut into pieces). They acquired pressure-volume curves that they used to estimate the Young's modulus value. The estimates acquired were based on adjusting the Young's modulus of a simplified mathematical model proposed by them so that predicted pressure-volume curves matched their measurements. They simplified the model by assuming that the undeformed eardrum can be represented by a flat circular membrane and they omitted the manubrium and pars flaccida from their model. They determined the Young's modulus to be 10.33 MPa and 6.88 MPa for old subjects and young subjects, respectively. Their values are lower than those measured by others, and Gaihede *et al*, (2007) argue that their values are based on *in vivo* measurements as opposed to measurements based on cadaveric samples as done by others. Because their measurements are made *in vivo*, they

feel that a larger thickness value can be used in their model. Presumably, this increase in thickness results in a smaller estimated Young's modulus. However, the accuracy of their reported values may be significantly affected by the rough approximation of eardrum geometry used in their work.

One method that can in principle be applied to intact eardrums is the indentation technique described by Samani *et al*, (2003). Very recently, Hesabgar *et al*, (2010) estimated the Young's modulus value of rat eardrums using this indentation technique. The average "effective" Young's modulus value reported by them for seven rats was 21.7 MPa  $\pm$  1.2 MPa. Like Gaihede *et al*, (2007), Hesabgar *et al*, (2010) fit modeling results to experimentally measured load-displacement curves. Unlike Gaihede *et al*, (2007), Hesabgar *et al*, (2010) used a model that included the 3-dimensional shape of the eardrum and included the manubrium and the pars flaccida in addition to the pars tensa. Geometric nonlinearity was also taken into account. The main advantage of the technique presented by Hesabgar *et al*, (2010) is that strips do not have to be cut from the eardrum. Aernouts *et al*, (2010) also estimated the eardrum elasticity *in situ*. They performed indentation testing like Hesabgar *et al*, (2010) and measured the elasticity under the assumption that the pars tensa is linear, homogenous elastic material. Their estimates are higher than that of all other researchers, suggesting that their eardrums had dehydrated and become stiffer due to specimens' surface exposure.

The indentation techniques used by Hesabgar *et al*, (2010) and Aernouts *et al*, (2010) require that the tip of the indenter be perpendicular to the point of contact on the eardrum to minimize slipping of the indenter. Jahromi (2010) presented a technique in which the eardrum was pressurized and the shape of the deformed eardrum was measured. The

Young's modulus in an FE model of the eardrum similar to that of Hesabgar *et al*, (2010) was then optimized so that simulated pressurized eardrum shapes matched the measured shapes. They reported an average "effective" Young's modulus value of  $22.8 \text{ MPa} \pm 1.5 \text{ MPa}$  for the six rat specimens used in their study.

#### **1.4.2. Previous eardrum mechanics works under the assumption of orthotropy**

The ultrastructure of the pars tensa suggests that it may be better modeled as an orthotropic material. Most previous work on quantifying orthotropy of the pars tensa involves estimating the Young's modulus in the radial direction and in the circumferential direction.

Luo *et al*, (2009) estimated the Young's modulus of the eardrum in the radial and circumferential directions over a range of strain rates. They found that value of the Young's modulus increases with increasing the strain rate because of the viscoelastic properties of the eardrum. They investigated the mechanical properties of the human eardrum at high strain rates. They reported that the Young's modulus of the normal human eardrum varies from 45.2 to 58.9 MPa in the radial direction, and it varies from 34.1 to 56.8 MPa in the circumferential direction for strain rates between 300 to  $2000 \text{ s}^{-1}$ . Furthermore, they reported that the Young's modulus in the radial direction is larger than the Young's modulus in the circumferential direction for the same strain rate. As noted in Section 1.4.1, cutting the eardrum presents challenges.

### **1.5. Objective**

Because of the importance of the mechanical properties of the eardrum in FE modeling and the lack of estimates of the orthotropic properties of the eardrum on intact

samples, the focus of this thesis is on estimating the orthotropic elastic properties of the eardrum based on methods that do not involve cutting the eardrum. In particular, the indentation method of Hesabgar *et al*, (2010) and the pressurization method of Jahromi (2010) were extended to estimate the orthotropic elastic parameters. These techniques were extended by modeling the eardrum as an orthotropic material and using the models in an optimization framework as done before but this time to estimate the orthotropic elastic parameters from measured indentation and pressurization data. The feasibility of both techniques was first tested on synthetic computer-generated data with known “ground truth” values. The extended optimization approach was then applied to indentation measurements on the rat eardrum made by Hesabgar *et al*, (2010) as these data were readily available. Chapter 2 is a complete manuscript that describes the methodology, testing and application to rat eardrums. Chapter 3 presents conclusions and future directions.

## 1.6. References

- Aernouts, J., Soons, J.A., Dirckx, J.J., 2010. Quantification of tympanic membrane elasticity parameters from in situ point indentation measurements: Validation and preliminary study. *Hear. Res.*, 263(1-2), 177-182.
- Akache, F., Funnell, W.R., Daniel, S.J., 2007. An experimental study of tympanic membrane and manubrium vibrations in rats, *Audiol. Neurootol.* 12 49-58.
- Beer, H.-J., Bornitz, M., Hardtke, H.-J., Schmidt, R., Hofmann, G., Vogel, U., Zahnert, T., Hüttenbrink, K.-B., 1999. Modelling of components of the human middle ear and simulation of their dynamic behavior. *Audiol. Neuro-otol.*, 4 (3-4) 156-162.
- Békésy, G.v., 1960. *Experiments in Hearing*, McGraw-Hill, Toronto, ON.
- Castagno.L.A., Lavinsky.L., 2006. Tympanic membrane healing in myringotomies performed with argon laser or microknife: an experimental study in rats, *Rev Bras Otorrinolaringol.*, 72(6) 794-799.
- Cheng, T., Dai, C., Gan, R.Z., 2007. Viscoelastic properties of human tympanic membrane. *Ann. Biomed. Eng.*, 35 (2) 305-314.
- Daniel, S.J., Funnell, W.R.J., Zeitouni, A.G., Schloss, M.D., Rappaport, J., 2001. Clinical applications of a finite-element model of the human middle ear. *J. Otolaryngol.* 30 (6), 340-346.
- Daphalapurkar, N.P., Dai, C., Gan, R.Z., Lu, H., 2009. Characterization of the linearly viscoelastic behavior of human tympanic membrane by nanoindentation. *J. Mech. Behav. Biomed. Mater.*, 2 (1) 82-92.
- Decraemer, W.F., Dircks, J.J.J., Funnell, W.R.J., 1991. Shape and derived geometrical parameters of the adult, human tympanic membrane measured with a phase-shift moiré interferometer., *Hear.Res.* (51) 107-121.
- Decraemer, W.F., Maes, M.A., Vanhuyse, V.J., 1980. An elastic stress-strain relation for soft biological tissues based on a structural model. *J. Biomech.*, 13 (6) 463-468.
- Dirckx, J., Decraemer, W., 1989. Phase-shift moiré apparatus for automatic 3D surface measurement. *Review of Scientific Instruments* 60, 3698–3701.
- Donaldson J.A., Duckert L.G., Lampert P.M., Rubel E.W., 1992. *Surgical Anatomy of the Temporal Bone*, 4th ed. (Raven Press, New York)
- Durrant, J.D., Lovrinic, J.H., c1977. *Bases of hearing science* John D. Durrant and Jean H. Lovrinic. -, Baltimore : Williams & Wilkins,.
- Eiber, A., 1999. Mechanical modeling and dynamical behavior of the human middle ear. *Audiology and Neurotology* 4, 170–177.

- Eiber, A., Breuninger, C., Jorge, J., Zenner, H., Maassen, M., 2006. On the optimal coupling of an implantable hearing aid – measurements and simulations. In: Eiber, A., Huber, A. (Eds.), *Proceedings of the 4th Int. Symposium: Middle Ear Mechanics in Research and Otology*. World Scientific Publishing Co. Pte. Ltd., Singapore, 246–252.
- Elkhoury, N., Liu, H., Funnell, W.R.J., 2006. Low-frequency finite-element modeling of the gerbil middle ear. *JARO* 7, 399–411.
- Fay, J.P., Puria, S., Steele, C.R., 2006. The discordant eardrum, *Proc.Natl.Acad.Sci.U.S.A.* 103, 19743-19748.
- Fay, J.P., Puria, S., Decraemer, W.F., Steele, C., 2005. Three approaches for estimating the elastic modulus of the tympanic membrane. *J. Biomech.*, 38 (9) 1807-1815.
- Ferris, P., Prendergast, P.J., 1999. Middle-ear dynamics before and after ossicular replacement. *J. Biomech.* 33 (5), 581–590.
- Fung, Y.C., 1993. *Biomechanics: Mechanical Properties of Living Tissues*, 2<sup>nd</sup> ed., Springer-Verlag, New York City, NY.
- Funnell, W.R.J., 1975. *A Theoretical Study of Eardrum Vibrations Using the Finite-Element Method*. Ph.D. thesis, McGill University, Montreal, x + 199 pp. Updated 1976. Available from the author, or on microfilm from the National Library of Canada.
- Funnell, W.R.J., and Laszlo, C.A., 1975. Modelling the eardrum as a doubly curved shell using the finite-element method. *J. Acoust. Soc. Am.* 57 Suppl: 72.
- Funnell, W.R.J., Laszlo, C.A., 1978. Modeling of the cat eardrum as a thin shell using the finite- element method. *J. Acoust. Soc. Am.*, 63 (5) 1461-1467.
- Gaihede, M., Liao, D., Gregersen, H., 2007. In vivo areal modulus of elasticity estimation of the human tympanic membrane system: modelling of middle ear mechanical function in normal young and aged ears. *Phys. Med. Biol.*, 52 (3) 803-814.
- Gan, R., Sun, Q., Feng, B., Wood, M., 2006. Acoustic-structural coupled finite element analysis for sound transmission in human ear – pressure distributions. *Medical Engineering & Physics* 28, 395–404.
- Hellstrom, S., Salen, B., Stenfors, L., 1982. Anatomy of the rat middle ear. *Acta Anat (Basel)*, (112) 346-52.
- Hesabgar, S.M., Marshall, H., Agrawal, S. K., Samani, A., Ladak, H.M., 2010. Measuring the quasi-static Young's modulus of the eardrum using an indentation technique. *Hear. Res.*, 263(1-2), 168-176.
- Huang, G., Daphalapurkar, N.P., Gan, R.Z., Lu, H., 2008. A Method for measuring linearly viscoelastic properties of human tympanic membrane using nanoindentation. *J. Biomech. Eng.*, 130 (1) 014501.



- Jahromi, S.N.G., Estimation of the quasi-static Young's modulus of the rat eardrum using a pressurization method, School of Graduate and Postdoctoral Studies, University of Western Ontario, London, Ont., 2009.
- Kirikae, I., 1960. The Structure and Function of the Middle Ear. University of Tokyo Press, Tokyo.
- Koike, T., Wada, H., Kobayashi, T., 2002. Modeling of the human middle ear using the finite-element method. *Journal of the Acoustical Society of America* 111, 1306–1317.
- Kuypers, L.C., Decraemer, W.F., Dirckx, J.J., 2006. Thickness distribution of fresh and preserved human eardrums measured with confocal microscopy. *Otology & Neurotology* 27, 256–264.
- Ladak, H.M., Funnell, W.R.J., Decraemer, W.F., Dirckx, J.J.J., 2006. A geometrically nonlinear finite-element model of the cat eardrum. *J. Acoust. Soc. Am.*, 119 (5) 2859-2868.
- Lee, C.F, Chen, J.H., Chou, Y.F., Hsu, L.P., Chen, P.R., Liu, T.C., 2007. Optimal graft thickness for different sizes of tympanic membrane perforation in cartilage myringoplasty: a finite element analysis, *Laryngoscope*. 117 725-730.
- Lee, C.F., Hsu, L.P., Chen, P.R., Chou, Y.F., Chen, J.H, Liu, T.C., 2006. Biomechanical modeling and design optimization of cartilage myringoplasty using finite element analysis, *Audiol.Neurootol.* 11 380-388.
- Lim, D. J., 1995. Structure and function of the tympanic membrane: a review. *Acta Oto-Rhino Laryngologica Belgica* 49 2 101-15.
- Luo, H., Dai, C., Gan, R.Z., Lu, H., 2009. Measurement of young's modulus of human tympanic membrane at high strain rates. *Journal of Biomechanical Engineering* 131, 064501-1.8.
- Mohammed, A., 2005. Computational elasticity: theory of elasticity and finite and boundary element methods. Alpha Science Int'l Ltd., 33-66.
- Samani, A, Bishop, J, Luginbuhl, C., Plewes, D. B., 2003. Measuring the elastic modulus of ex vivo small tissue samples *Phys. Med. Biol.* 48 14 2183-98.
- Sun, Q., Gan, R., Chang, K., Dormer, K., 2002. Computer-integrated finite element modeling of human middle ear. *Biomechanics and Modeling in Mechanobiology* 1, 109–122.
- Tuck-Lee, J.P., Pinsky, P.M., Steele, C.R., Puria, S., 2008. Finite element modeling of acousto-mechanical coupling in the cat middle ear. *J. Acoust. Soc. Am.*, 124 (1) 348-362.

Vander, A.J., Sherman, J.H., and Luciano, D.S., 2004. HUMAN PHYSIOLOGY: The Mechanisms of Body Function. Ninth Edition (McGraw Hill, Sydney).

Zahnert, T., Huttenbrink, K.B., Murbe, D., Bornitz, M., 2000. Experimental investigations of the use of cartilage in tympanic membrane reconstruction, Am.J.Otol. 21 322-328.

Zimmer, W.M., Deborah, F.R., Saunders, J.C., 1994. Middle-ear development VI: Structural maturation of the rat conducting apparatus. Anatomical Record 239: 475-484.

## Chapter 2

### Estimation of the Orthotropic Elastic Properties of the Rat Eardrum

(Prepared for Submission to: The Journal of Medical and Biological Engineering)

#### 2.1. Introduction

Finite-element (FE) modeling of the eardrum is an active area of research with several groups publishing models even in the last three years (Daphalapurkar *et al*, 2009; Gan *et al*, 2009; Liu Hou-guang *et al*, 2009; Yao Wen-juan *et al*, 2009; Aernouts *et al*, 2010; Hesabgar *et al*, 2010; Zhu *et al*, 2010; Gentil *et al*, 2011; Vollandri *et al*, 2011; Wang *et al*, 2011). Well validated models could potentially be used for testing new surgical procedures and refining audiological tests of middle-ear function (Daniel *et al*, 2001). However, the accuracy of these models depends critically on a number of input modeling parameters including the shape of the individual eardrum, its thickness and its mechanical properties (Funnell and Laszlo, 1978). Subject-specific shapes have been accurately measured using moiré profilometry (e.g., Decraemer *et al*, 1991), a non-contacting optical technique, and more recently using micro-computed tomography (Tuck-Lee *et al*, 2008). Thickness has also been measured in gerbils (Kuypers *et al*, 2005b), cats (Kuypers *et al*, 2005a) and human (Kuypers *et al*, 2006).

A number of investigators have recently started refining measurements of the mechanical properties of the eardrum. Particular focus has been made to estimate the properties of the pars tensa of the eardrum because it is the main determinant of the impedance matching function of the middle ear. Several authors have modeled the pars

tensa as a homogeneous linearly elastic *isotropic* thin shell. Such a material can be characterized by its Young's modulus and its Poisson's ratio. Typically, a Poisson's ratio of 0.3 is assumed in modeling studies (Funnell and Laszlo, 1978), and effort has focused on estimating the Young's modulus of the pars tensa (Aernouts *et al*, 2010; Daphalapurkar *et al*, 2009; Huang *et al*, 2008; Gaihede *et al*, 2007; Cheng *et al*, 2007; Decraemer *et al*, 1980; Kirikae, 1960; Békésy 1960).

Fay *et al*, (2006) indicate that an isotropic model can only be used to model the mechanical behavior of the eardrum over a limited range of frequencies. For example, if a Young's modulus of 30 MPa is used to model the pars tensa, simulated frequency responses only match measured responses up to about 1.5 kHz. Above that frequency, the mismatch between simulation and measurement is significant. If a Young's modulus of 100 MPa is used, simulations better match measurements at high frequencies (above 1.5 kHz); however, a mismatch now occurs at low frequencies. A single Young's modulus cannot be found for an isotropic model that allows modeling results to match experimental data at all frequencies. If the pars tensa is modeled as an *orthotropic* material, then simulation results match measurements at all frequencies using a single set of orthotropic elastic parameter values: There is no need to adjust the values based on frequency (Fay *et al*, 2006). An orthotropic material model is justified based on the fibrous ultrastructure of the eardrum.

Indeed, the same group has attempted to estimate the Young's modulus of the eardrum in the radial and circumferential directions by using three methods: (1) constitutive modeling using experimental observations of radial and circumferential fiber densities, (2) re-examining previously published tensile testing and beam-bending

experiments, and (3) performing their own dynamic measurements and adjusting the parameters of a fibrous composite shell model of the eardrum so simulations match measurements. Using these approaches, *bounds* were determined for the elastic moduli. The recent work of Luo *et al* (2009) refines these bounds through the use of tensile testing of strips cut along the radial and along the circumferential directions. However, tensile testing has a number of technical challenges. Apart from the issue of compromising the tissue's structural integrity, to minimize the effects of boundary conditions on the measurement's accuracy, tensile tests typically require a significant volume of homogeneous tissue (Samani *et al* 2003). However, both the fiber density (Lim *et al* 1968; Lim *et al* 1970) and thickness (Kuypers *et al*, 2006; Kuypers *et al*, 2005a; Kuypers *et al*, 2005b) of the eardrum can vary over a matter of millimeters. Furthermore, the eardrum is remarkably delicate, has a complex geometry, and is relatively difficult to extract. All of these factors contribute to the difficulty of conducting a uniaxial tension test, hence impacting its accuracy.

*In situ* methods have been developed that allow one to estimate the properties of the eardrum while it is intact and is attached to the ear canal, i.e., no strips need to be cut. Hesabgar *et al* (2010) present one such method in which the Young's modulus of an FE model of the rat eardrum with subject-specific geometry is numerically optimized to produce a match between simulated force-displacement curves and those acquired experimentally through indentation testing. The optimal value is then taken to be the actual Young's modulus of the pars tensa under test. A similar indentation-based method was developed by Aernouts *et al* (2010). Recognizing the challenges of indentation testing and modeling of indentation experiments, Jahromi (2010) developed a

pressurization-based method in which the acquired data consisted of measurements of the deformed shape of the eardrum after applying a sequence of static pressures. As with Hesabgar *et al* (2010), the Young's modulus was estimated by optimizing its value in the model until simulated responses matched experimental measurements.

Both the indentation-based method and the pressurization-based *in situ* methods assumed that the pars tensa can be modeled as a linear elastic homogeneous isotropic material and can thus be characterized by a single Young's modulus ( $E$ ) and a Poisson's ratio ( $\nu$ ). The objective of this work is to extend the indentation-based method of Hesabgar *et al* (2010) and the pressurization-based method of Jahromi (2010) by modeling the eardrum as a homogeneous linear elastic orthotropic material and estimating the orthotropic elastic properties of the eardrum by numerical optimization of an FE model of the eardrum. Four independent in-plane elastic parameters need to be determined for modeling thin orthotropic materials such as the pars tensa. These are the longitudinal ( $E_x$ ) and transverse ( $E_y$ ) Young's moduli, the in-plane shear modulus ( $G_{xy}$ ), and the Poisson's ratio. By using the commonly accepted value of 0.3 for the Poisson's ratio, the problem reduces to estimating  $E_x$ ,  $E_y$  and  $G_{xy}$  for the pars tensa. The feasibility of both techniques was first tested on *synthetic* computer-generated data with known "ground truth" values and with various levels of added noise. One of the extended optimization approaches was then applied to indentation measurements of the rat eardrum made by Hesabgar *et al* (2010) as these data were readily available.

## 2.2. Materials and Method

### 2.2.1. Overview

Figure 2.1 shows a flowchart that describes both the extended indentation-based algorithm and the extended pressurization-based algorithm. The input to both estimation algorithms consists of a subject-specific 3D FE mesh of the eardrum under test and its corresponding experimental response data. Response data are force-displacement curves for the indentation-based algorithm and pressurized shape measurements for the pressurization-based algorithm. The method for constructing the 3D FE mesh is the same for both algorithms and is described in Section 2.2.

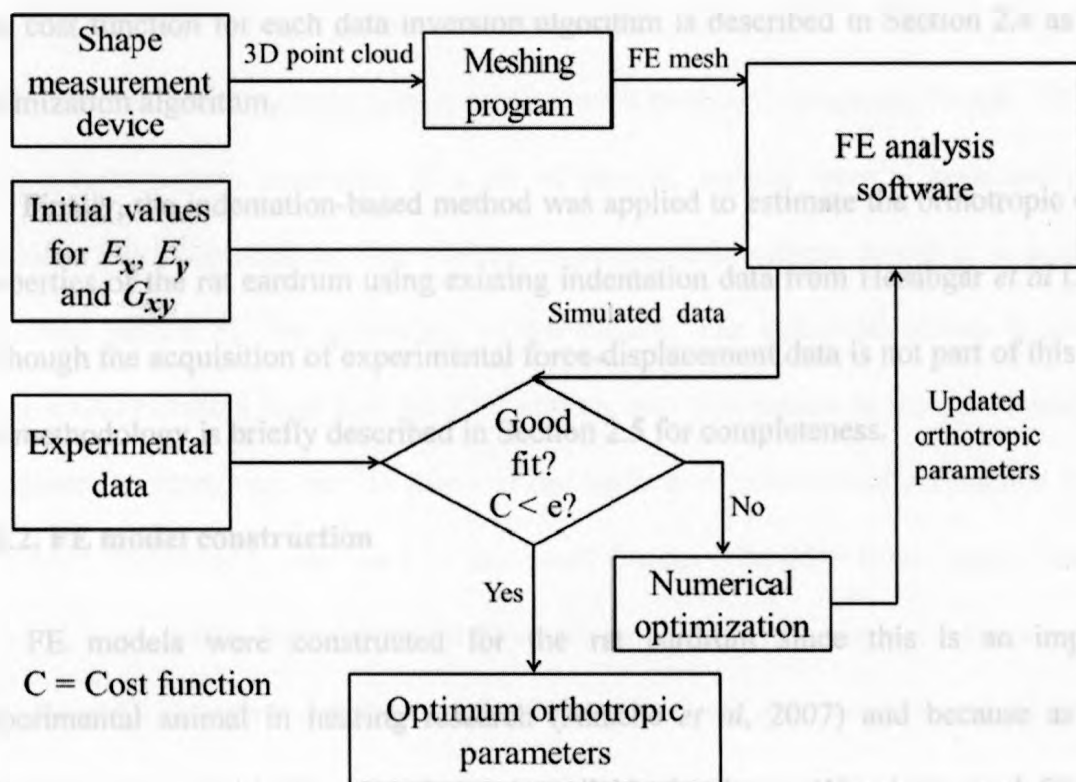


**Figure 2.1** The estimation flowchart. Flowchart describing both the indentation-based and pressurization-based methods for estimating the eardrum's orthotropic elastic parameters

The optimization framework described by Figure 2.1 requires experimental data to which simulation results are matched. To test the fidelity of the proposed optimization based data inversion algorithms, the two methods were first tested on *synthetic* computer-generated data. For the indentation-based algorithm, these consisted of force-displacement curves, whereas for the pressurization-based algorithm, these consisted of the deformed shape of the eardrum at specific pressures. The approach used for generating synthetic response data for both methods is described in Section 2.3.

In order to find the eardrum's orthotropic parameters using either the indentation-based method or the pressurization-based method, a cost function is optimized such that the response simulated using these parameter values match the synthetic response data. The cost function for each data inversion algorithm is described in Section 2.4 as is the optimization algorithm.

Finally, the indentation-based method was applied to estimate the orthotropic elastic properties of the rat eardrum using existing indentation data from Hesabgar *et al* (2010). Although the acquisition of experimental force-displacement data is not part of this work, the methodology is briefly described in Section 2.5 for completeness.

### **2.2.2. FE model construction**

FE models were constructed for the rat eardrum since this is an important experimental animal in hearing research (Akache *et al*, 2007) and because as noted above, experimental indentation data are available for the rat (Hesabgar *et al*, 2010). In order to construct an FE model of a rat eardrum, the 3D shape of the eardrum is required because the shape of the eardrum is important to its mechanical function (Funnell and



Laszlo, 1978; Fay *et al.*, 2006). Shape data were used from the study of Hesabgar *et al.* (2010). In that study, healthy eardrums from adult Sprague Dawley rats were used. The rats were euthanized in accordance with the University of Western Ontario's Animal Use Subcommittee. For each rat, the temporal bone was removed 30 min post mortem. The ear canal was resected to within 0.5 mm of the eardrum in order to obtain a good view of the eardrum for shape measurement. To measure the mechanical response of the eardrum without the confounding effects of the ossicular and cochlear loads, the malleus was immobilized by gluing the malleolar head to the middle-ear wall as described elsewhere (Ladak *et al.*, 2004). The eardrum was left intact, i.e., the eardrum was not dissected from its attachments to the ear canal or the manubrium of the malleus.

The 3D shape of each eardrum was measured using Fourier transform profilometry (FTP), which is a non-contact optical measurement method (Takeda and Mutoh, 1983). In FTP, a light pattern consisting of a set of parallel vertical lines is projected onto a diffusely reflecting surface. The surface modulates this pattern, resulting in a slightly deformed pattern of lines appearing on the surface. The deformed pattern is acquired using a CCD camera built into the FTP system, and this pattern is then processed by a computer to reconstruct the 3D shape of the surface. A commercially available Fourier transform profilometer was used in this work (model MM-25D from Opton Company Limited, Seto, Aichi, Japan). This profilometer has a spatial measurement accuracy of 10  $\mu\text{m}$ . Since FTP requires a diffusely reflecting surface with good contrast and the eardrum is transparent, a thin white coating was applied to the eardrum. Specifically, a spray-on coating was used (Spotcheck SKD-S2 Developer, Magnaflux, Glenview, IL). The effects of similar coatings on shape measurements have been shown to be negligible (Dirckx and

Decraemer, 1997). The output of the profilometer is a cloud of points representing the surface being measured.

In order to form an FE mesh from this cloud of points, the Trans-Finite Interpolation (TFI) technique (Knupp and Steinberg, 1993) was used. In its simplest form, TFI warps a unit square with a mesh of quadrilateral elements as shown in Figure 2.2 into an arbitrary shape, thus producing a quadrilateral mesh for the arbitrary shape. In terms of FE analysis, quadrilateral elements as used here have better performance compared to triangular elements used in other studies (e.g., Funnell and Laszlo, 1978).

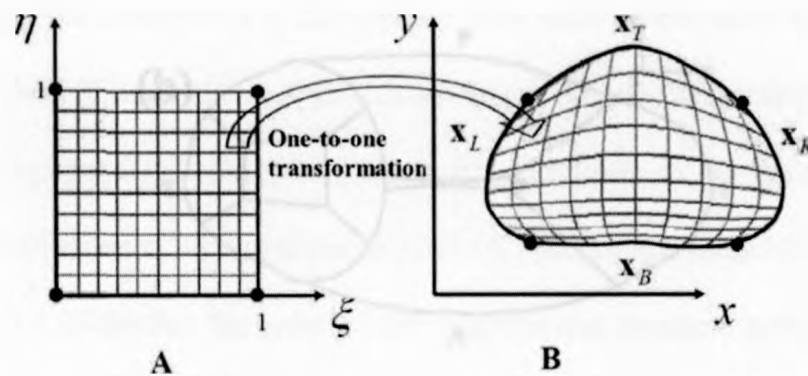


**Figure 2.2** Illustration of basic TFI meshing algorithm. A one-to-one transformation from a unit square with a quadrilateral mesh to an arbitrary shape is shown. This figure is a reproduction from a figure in Curtis *et al* (2007) with some changes.

The eardrum has a complex shape with several sub-surfaces (pars tensa, pars flaccida, and manubrium), so the simple TFI method described by Figure 2.2 cannot be used directly to produce a mesh for the eardrum. Instead, the TFI method was applied to simpler zones defined on the eardrum as described here. When applying TFI to the eardrum, a 2D line drawing of the specific eardrum needs to be created in which the following boundaries are demarcated: the tympanic ring, the pars tensa, the pars flaccida, the ligament separating the pars tensa from the pars flaccida, and the manubrium. These

boundaries were traced manually from a high resolution digital image of same eardrum under test. This step of mesh construction is shown in Figure 2.3(a).

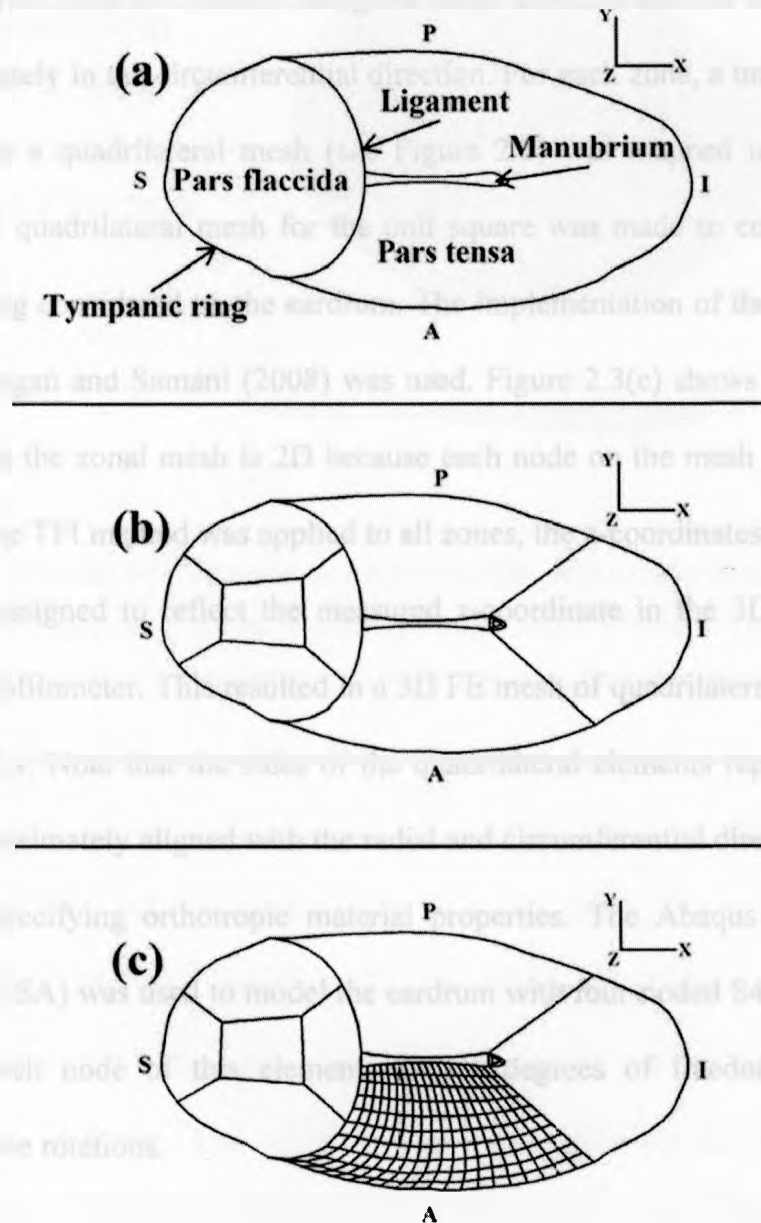


**Figure 2.3** Three basic steps for generating an FE mesh of the eardrum using the TFI technique. (a) Boundaries of the tympanic ring, the pars tensa, the pars flaccida, the ligament separating the pars tensa from the pars flaccida, and the manubrium were traced manually in 2D from a high resolution digital image of the eardrum. (b) The 2D line sketch of the eardrum was decomposed into fourteen zones. (c) Each zone was meshed using the basic TFI algorithm. Only the mesh for one of the fourteen zones is shown.

Next, the 2D line drawing was decomposed into fourteen zones. This step is shown in Figure 2.3(b). Each zone can be described as a quadrilateral with possibly curved sides. On the pars tensa, two sides are directed along the radial direction and the remaining two sides are approximately in the circumferential direction. For each zone, a unit square that is decomposed into a quadrilateral mesh (see Figure 2.2) was mapped using the TFI method so that the quadrilateral mesh for the unit square was made to conform to the particular zone being considered on the eardrum. The implementation of the TFI method developed by O'Hagan and Samani (2008) was used. Figure 2.3(c) shows the mesh for one zone. Note that the zonal mesh is 2D because each node on the mesh has a zero z-coordinate. Once the TFI method was applied to all zones, the z-coordinates of each node of the mesh was assigned to reflect the measured z-coordinate in the 3D point cloud produced by the profilometer. This resulted in a 3D FE mesh of quadrilateral elements as shown in Figure 2.4. Note that the sides of the quadrilateral elements representing the pars tensa are approximately aligned with the radial and circumferential directions, which is necessary for specifying orthotropic material properties. The Abaqus FE software (Simulia Inc., RI, USA) was used to model the eardrum with four-noded S4 quadrilateral shell elements. Each node of this element has six degrees of freedom, i.e., three translations and three rotations.

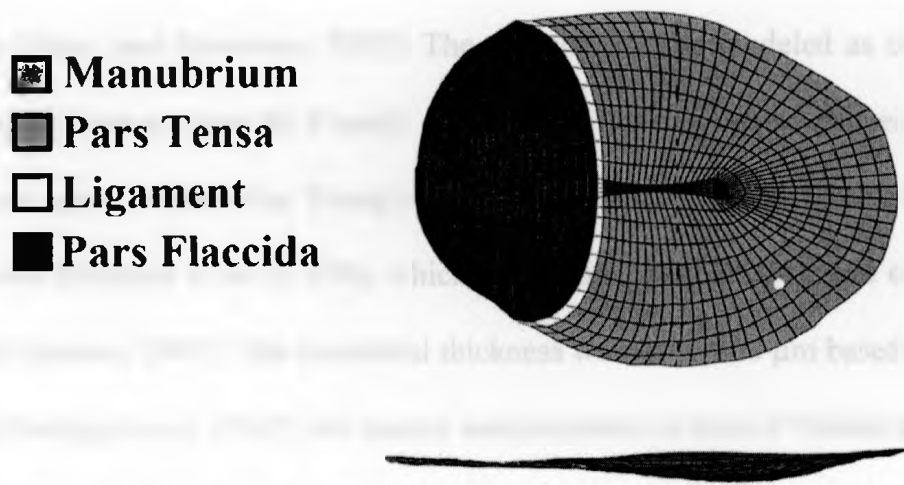


**Figure 2.4** A typical FE mesh for a rat eardrum. (a) View of FE mesh as seen from the ear canal. Also, the position of the indenter is shown by a dot. (b) View normal to view a. The anterior (A), posterior (P), superior (S) and inferior (I) directions are indicated in view (a).

To enable simulation, all parameters of the FE model were set to values from the literature except for the orthotropic elastic parameters of the pars tensa ( $E_x$ ,  $E_y$ , and  $G_{xy}$ ) which needed to be optimized. The optimization algorithm sets  $E_x$ ,  $E_y$ , and  $G_{xy}$  to some arbitrary initial values and then refines them. The thickness of the pars tensa was measured from a micro-CT image and an average value of 12  $\mu\text{m}$  was assigned to the model (Hesabgar *et al*, 2010). The same thickness was taken for the pars flaccida. Furthermore, the pars flaccida was assumed to be isotropic and more compliant than the pars tensa. Its Young's modulus was constrained to be equal to one-fortieth of the sum of the longitudinal and the transverse Young's moduli of the pars tensa. This constraint on the Young's modulus values of the pars flaccida was an arbitrary modeling choice to make the pars flaccida model more compliant than the pars tensa model. The ligament

separating the pars tensa from the pars flaccida was modeled as having a thickness of 12  $\mu\text{m}$ . Its Young's modulus was taken to be 100 MPa, which is the same as that of other ligaments (Ethier and Simmons, 2007). The manubrium was modeled as consisting of dense cortical bone as done by Funnell *et al* (1992). As they stated in their work, this provides an upper limit on the Young's modulus value of the manubrium. Its Young's modulus was assumed to be 15 GPa, which is the same as that of typical cortical bone (Mow and Huijkes, 2005). The manubrial thickness was set to 100  $\mu\text{m}$  based on a micro-CT scan (Hesabgar *et al*, 2010). All tissues were assumed to have a Poisson's ratio equal to 0.3. The tympanic ring was assumed to be fully clamped as was the superior boundary of the manubrium. However, the rest of the manubrium was tightly coupled to the eardrum and was free to move with it. This condition approximately simulates the experimental condition of immobilizing the malleolar head as in indentation testing.

### 2.2.3. Generating Synthetic Data

The FE mesh described in Section 2.3 was used in generating synthetic data to test both the indentation-based and pressurization-based estimation methods. Specifically, "ground truth values" of  $E_x = 20$  MPa,  $E_y = 34$  MPa, and  $G_{xy} = 12$  MPa were assumed.  $E_x$  and  $E_y$  were selected based on the circumferential and radial Young's moduli reported by Gan *et al*, (2006). The value of  $G_{xy}$  was arbitrarily set at 12 MPa. Henceforth, this model with ground truth parameter values will be referred to as the "ground truth model". Another model generated from the same shape data but with different arbitrary initial parameter values was then optimized using the techniques described in Section 2.4.

The indentation experiment of Hesbgar *et al* (2010) was simulated using the ground truth model. In that experiment, a point on the anterior pars tensa (indicated by the dot in Figure 2.4) was indented with spherical-ended indenter with a diameter of 0.5 mm. To simulate the experiment of Hesabgar *et al* (2010), the indenter was modeled as a rigid body and using small-slipping contact modeling. The indenter was used to indent the eardrum up to 90  $\mu\text{m}$  in steps of 9  $\mu\text{m}$ . At each step, the reaction force was computed by using the Abaqus FE software. Furthermore, because the amount of displacement in the indentation experiment was significant compared to the eardrum's thickness, the FE model incorporated geometric nonlinearity.

To generate synthetic data for the pressurization-based method of Jahromi (2010), pressures were applied to the model eardrum in steps of 0.5 KPa to a maximum of 4 KPa. At each pressurization step, the deformed shape of the eardrum was calculated using Abaqus with the inclusion of geometric nonlinearity to account for the large deformations.

Additionally, zero-mean Gaussian noise was added to each synthetic data set. Various levels of noise were used to achieve Signal-to-Noise Ratio (SNR) values of 2, 10, 100 and 200.

#### **2.2.4. Optimization**

For each of the methods (indentation or pressurization), a specific cost function with  $E_x$ ,  $E_y$ , and  $G_{xy}$  as the independent variables was formulated such that minimizing this cost function resulted in a match between simulation results and the response data. The optimal values of  $E_x$ ,  $E_y$ , and  $G_{xy}$  were taken to estimate the actual parameter values for the eardrum under test. For validation, only synthetic data generated using the ground

truth model were used. For the indentation-based method, the orthotropic elastic parameters were sought that produce the best match between the simulated force-displacement curve and corresponding synthetic response data. The cost function  $C_{in}$  for the indentation method is defined as the sum-of-squared reaction force differences between simulated and response data leading to the following constrained optimization problem:

$$C_{in}(E_x, E_y, G_{xy}) = \sum_{i=1}^{n_1} (f_i^{data} - f_i^{sim}(E_x, E_y, G_{xy}))^2 \quad (2-1)$$

Minimize  $C_{in}(E_x, E_y, G_{xy})$

$$\text{Subject to } \begin{cases} E_{xL} \leq E_x \leq E_{xU} \\ E_{yL} \leq E_y \leq E_{yU} \\ G_{xyL} \leq G_{xy} \leq G_{xyU} \end{cases}$$

where  $f_i^{data}$  and  $f_i^{sim}$  denote the ground truth reaction force and simulated reaction force, respectively, for point  $i$  along the force-displacement curve. Note that  $f_i^{sim}$  is a function of the variables to be optimized ( $E_x$ ,  $E_y$ , and  $G_{xy}$ ), and is calculated at each iteration of the optimization algorithm using the FE model and the current values of  $E_x$ ,  $E_y$ , and  $G_{xy}$ . The number of points along the force-displacement curve is specified by  $n_1$ .  $E_{xL}$  and  $E_{xU}$  are lower and upper bounds of the longitudinal Young's modulus ( $E_x$ ), respectively.  $E_{yL}$  and  $E_{yU}$  are the lower and upper bounds of the transverse Young's modulus ( $E_y$ ), respectively.  $G_{xyL}$  and  $G_{xyU}$  are the lower and upper bounds of the in-plane shear modulus ( $G_{xy}$ ), respectively.

In the pressurization-based method, the cost function was designed so it was minimum when the values of  $E_x$ ,  $E_y$ , and  $G_{xy}$  were such that the match between the



simulated pressurized shape and the corresponding synthetic response data was best. The pressurization-based cost function  $C_p$  is defined at a particular pressure as the sum-of-squared nodal  $z$ -coordinate differences between simulated and response data leading to the following constrained optimization problem:

$$C_p(E_x, E_y, G_{xy}) = \sum_{i=1}^{n_2} (z_i^{data} - z_i^{sim}(E_x, E_y, G_{xy}))^2 \quad (2-3)$$

$$\text{Minimize } C_p(E_x, E_y, G_{xy})$$

$$\text{Subject to } \begin{cases} E_{xL} \leq E_x \leq E_{xU} \\ E_{yL} \leq E_y \leq E_{yU} \\ G_{xyL} \leq G_{xy} \leq G_{xyU} \end{cases}$$

where  $z_i^{data}$  and  $z_i^{sim}$  are the experimentally acquired and simulated surface shape  $z$ -coordinates, respectively. The number of the points on the surface is specified by  $n_2$ .

For both the indentation-based cost function and the pressurization-based cost function, the upper and lower limits were set to:  $E_{xU} = 72$  MPa,  $E_{yU} = 88$  MPa,  $G_{xyU} = 48$  MPa,  $E_{xL} = 7$  MPa,  $E_{yL} = 7$  MPa and  $G_{xyL} = 4$  MPa. Based on the available literature, the search space defined by these limits is very large.

Each cost function was minimized to find the optimal orthotropic elastic parameters using a variant of the Nelder-Mead simplex method (Lagarias *et al*, 1998). For the pressurization-based method, the minimization was done for each pressure, and the optimal values at each pressure were averaged to get the final result. The optimization process starts by using initial guesses for the orthotropic parameters and then systematically changes them until the minimum of the cost function is reached. To ensure

uniqueness and accuracy of results obtained from the optimization process, four significantly different sets of orthotropic parameters initial guesses were used. Table 1 shows these initial guess values sets.

**Table 1** Initial guess sets of orthotropic parameters used in the optimization process.

Initializing orthotropic parameter values		
$E_x$ (MPa)	$E_y$ (MPa)	$G_{xy}$ (MPa)
27.00	40.00	16.00
30.00	25.00	8.00
10.80	10.08	4.08
50.00	60.00	30.00

The optimization process was terminated when the tolerance for the cost function values and orthotropic parameter values were small enough. For the synthetic data, the tolerances were set to 10 Pa for  $E_x$ ,  $E_y$ , and  $G_{xy}$  and  $10^{-16}$  for either cost function. For the experimental indentation data (see next section), the tolerances were set to 100 Pa for  $E_x$ ,  $E_y$ , and  $G_{xy}$  and  $10^{-8}$  for either cost function.

### 2.2.5. Experimental indentation data

As mentioned previously, the indentation data of Hesabgar *et al* (2010) were used to estimate  $E_x$ ,  $E_y$ , and  $G_{xy}$  for actual rat eardrums. In their experiment, a spherical-ended indenter with a diameter of 0.5 mm was used. A spherical-ended indenter does not have sharp edges and does not result in tearing of the eardrum as does a plane-ended indenter. However, the contact area of a spherical-ended indenter grows gradually while the

indenter moves further down on the eardrum. The contact area growth characteristics depend on the geometry of the eardrum and the indenter in addition to their stiffness. To obtain the contact area incrementally throughout the indentation process, which is necessary for indentation force calculation, contact problem modeling is necessary. The indenter was applied perpendicular to the local eardrum surface in order to minimize slipping of the indenter with respect to the eardrum. The indenter descended until it just touched the surface of the eardrum and was then stopped. The point of contact was in the anterior pars tensa as shown in Figure 2.5 for one eardrum. Furthermore, the orientation of the eardrum was chosen such that the indenter was normal to the surface at the point of contact in order to avoid slippage between the eardrum and indenter. This was consistent with the small-slipping contact condition used in modeling of the eardrum (see Section 2.2). After applying several sinusoidal indentation cycles of loading and unloading for preconditioning, four similar cycles of sinusoidal indentation were applied to the specimen with a frequency of 0.5 Hz. Force-displacement data corresponding to the four cycles were recorded. The purpose of applying four cycles was to have enough cycles to choose the best one from them given that the quality of the force-displacement curve can be affected by random mechanical vibration or electrical noise.

For optimization, only the loading part of the best sinusoidal indentation cycle was used. The experimentally measured unloading part of the loading cycle was not used because of inaccuracy in the measured forces throughout the unloading phase of the cycle. As described by Samani *et al* (2003), this inaccuracy is due to discontinuity of contact between the indenter and the tissue during unloading.

## 2.3. Results

### 2.3.1 Algorithm testing on synthetic data

The ground truth values were recovered with both estimation techniques without any error in the absence of noise. Values of the in-plane shear modulus ( $G_{xy}$ ) recovered by the indentation-based and by the pressurization-based techniques are shown in Figure 2.5 and Figure 2.6, respectively, for various levels of zero-mean Gaussian noise. Initialization values, optimization algorithm parameters, and FE models are the same for both figures. As expected, these figures show that the recovered values are closer to the ground truth values with smaller levels of noise. The pressurization technique has an accuracy in excess of 90% when the SNR (signal-to-noise ratio) is 2 or greater. For the indentation technique, an SNR greater than 200 is required to achieve over 90% accuracy. The above estimation methods are valid over a wide range of initialization values used with the optimization algorithms from half the ground truth values to twice the ground truth values.

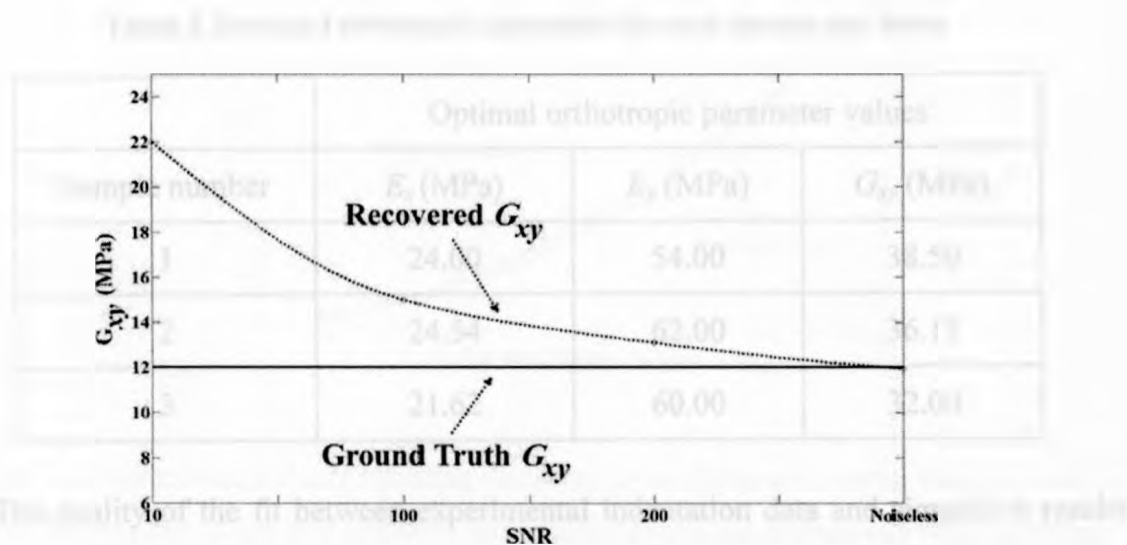


**Figure 2.5** Ground truth and recovered values of in-plane shear modulus for the indentation-based method applied to synthetic response data with different levels of Gaussian noise.

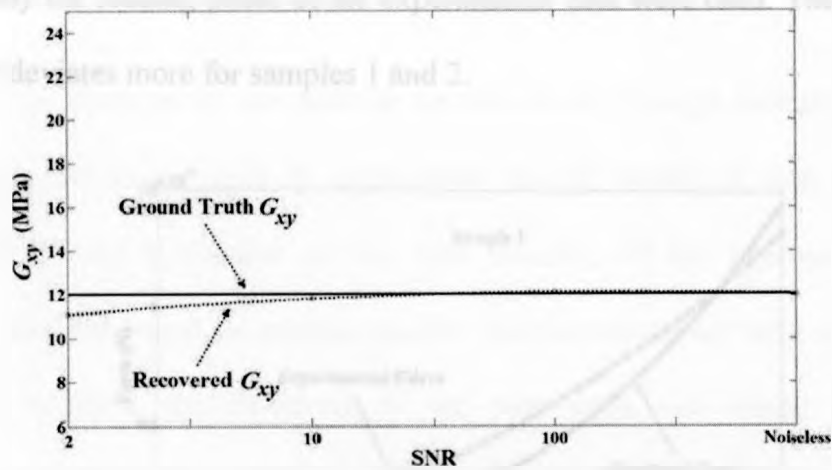


**Figure 2.6** Ground truth and recovered values of in-plane shear modulus for the pressurization-based method applied to synthetic data with different levels of Gaussian noise.

### 2.3.2. Estimate from actual indentation data

Table 2 shows the estimated values of  $E_x$ ,  $E_y$ , and  $G_{xy}$  for three of the rats used by Hesabgar *et al* (2010). The indentation-based algorithm was used because these authors provide indentation data. The average values orthotropic parameter values plus/minus standard deviation across all three rats were of  $E_x = 23.39 \pm 1.55$  MPa,  $E_y = 58.67 \pm 4.16$  MPa, and  $G_{xy} = 35.56 \pm 3.29$  MPa.

**Table 2** Estimated orthotropic parameters for each sample pars tensa.

Sample number	Optimal orthotropic parameter values		
	$E_x$ (MPa)	$E_y$ (MPa)	$G_{xy}$ (MPa)
1	24.00	54.00	38.50
2	24.54	62.00	36.17
3	21.62	60.00	32.00

The quality of the fit between experimental indentation data and simulation results using the optimal orthotropic parameter is shown in Figure 2.8 for each of the three rats.

Recall that only the loading phase of the experimental data were used. The fit is best for sample 3, but deviates more for samples 1 and 2.

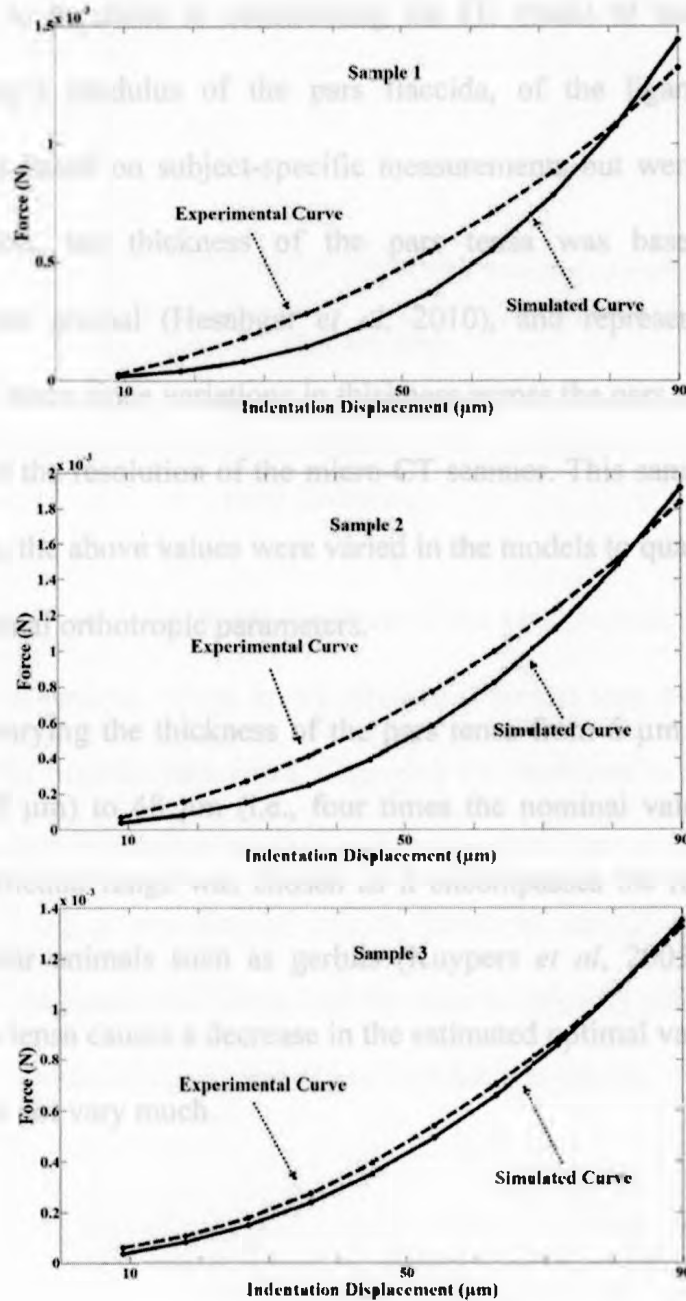


**Figure 2.7** Experimental and corresponding simulated force-displacement curve. Experimentally acquired loading part of one indentation cycle (dashed curve) in rat eardrums and corresponding simulated indentation response obtained from FE simulation (solid curve) with the corresponding optimal orthotropic elastic parameter values.

### 2.3.3. Variation of model parameters

Although the shape of the eardrum was known exactly through measurement, several approximations had to be made in constructing the FE model of each eardrum. The thickness and Young's modulus of the pars flaccida, of the ligament and of the manubrium were not based on subject-specific measurements but were taken from the literature. In addition, the thickness of the pars tensa was based on micro-CT measurements on one animal (Hesabgar *et al*, 2010), and represented the average thickness of the pars tensa since variations in thickness across the pars tensa could not be quantified because of the resolution of the micro-CT scanner. This same value was used for all animals. Thus, the above values were varied in the models to quantify their effects on the estimated optimal orthotropic parameters.

The effects of varying the thickness of the pars tensa from 6  $\mu\text{m}$  (i.e., 50% of the nominal value of 12  $\mu\text{m}$ ) to 48  $\mu\text{m}$  (i.e., four times the nominal value) are shown in Figure 2.8. This particular range was chosen as it encompasses the range of thickness values seen in similar animals such as gerbils (Kuypers *et al*, 2005). Increasing the thickness of the pars tensa causes a decrease in the estimated optimal values of  $E_x$  and  $E_y$ . By contrast,  $G_{xy}$  does not vary much.

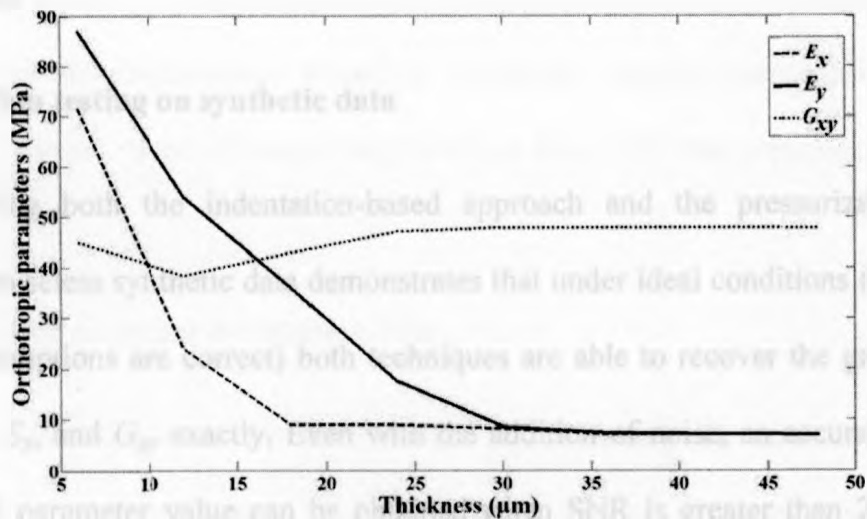


**Figure 2.8** Variation in optimal orthotropic parameters of the pars tensa as a function of the pars tensa thickness.

Varying the Young's modulus or the thickness of the pars flaccida does not have any effect on the estimated optimal values to two decimal places as long as the pars flaccida is kept more compliant than the pars tensa. Changing the thickness or Young's modulus of the ligament from half its value to twice its value does not affect the estimated optimal values of  $E_x$ ,  $E_y$ , and  $G_{xy}$  to two decimal places. Similarly, changing the thickness or Young's modulus of the manubrium from half its value to twice its value does not affect the estimated optimal values of  $E_x$ ,  $E_y$ , and  $G_{xy}$  to two decimal places.



## 2.4. Discussion

### 2.4.1. Algorithm testing on synthetic data

Applying both the indentation-based approach and the pressurization-based approach to noiseless synthetic data demonstrates that under ideal conditions (i.e., all FE modeling assumptions are correct) both techniques are able to recover the ground truth values of  $E_x$ ,  $E_y$ , and  $G_{xy}$  exactly. Even with the addition of noise, an accuracy of over 90% for each parameter value can be obtained when SNR is greater than 200 for the indentation-based method and greater than 2 for the pressurization-based method. In practice, such SNR values are easy to achieve as the amount of force data averaging that occurs during data acquisition to obtain each force value can be easily adjusted to increase the SNR. In indentation testing, 1000 samples are averaged when acquiring a single point on the force-displacement curve (Hesabgar *et al*, 2010). In the FTP system used by Jahromi (2010), up to 10 point clouds can be averaged to produce a single acquisition.

Nevertheless, the pressurization-based method has some advantages over the indentation-based method. When acquiring experimental force-displacement curves in indentation testing, the indenter must remain perpendicular to the local eardrum surface in order to minimize slipping. If a spherical indenter is used during the experiments to prevent damage to the eardrum, FE modeling becomes more complicated since the indentation test must be simulated as a contact problem. Using contact problem modeling is necessary because the area of contact between the indenter and eardrum grows as the indenter is initially pushed into the eardrum. The contact area's continuous growth

implies that the loading of the eardrum also changes continuously, hence conventional prescribed force or displacement boundary conditions become inappropriate in the respective FE model. None of these complications arise with the pressurization-based method.

#### 2.4.2. Application to actual indentation data

This work represents the first attempt at estimating the orthotropic elastic properties of the rat pars tensa. The longitudinal modulus ( $E_x$ ) corresponds to the circumferential fiber direction, whereas the transverse modulus ( $E_y$ ) corresponds to the radial fiber direction. As listed in Table 2,  $E_y$  is larger than  $E_x$ , which is consistent with the observation that the radial fibers are stiffer than the circumferential fibers (Funnell and Laszlo, 1982).

Luo *et al* (2009) have performed tensile testing on strips cut from the human eardrum, and they have investigated the effects of varying the strain rate. For strips cut in the radial direction, they modeled the strip as an *isotropic* material and estimated that the Young's modulus varies from 45.2 MPa to 58.9 MPa for strain rates varying from 300 to 2000  $s^{-1}$ . Note that the Young's modulus increases with increasing strain rate. The comparable value in the present work is  $E_y$ , which was estimated to be  $58.67 \pm 4.16$  MPa across the three rats. For strips cut in the circumferential, Luo *et al* (2009) estimated that the Young's modulus varies from 34.1 MPa to 56.8 MPa for strain rates varying from 300 to 2000  $s^{-1}$ . The comparable value in the present work is  $E_x$  which was estimated to be  $23.39 \pm 1.55$  MPa across the three rats. Although the values presented here cannot directly be compared mainly because of differences in species (rat vs. human) and

modeling assumptions (orthotropic vs. isotropic), it is interesting to note that the moduli were in similar ranges. Luo *et al* (2009) did not report an in-plane shear modulus ( $G_{xy}$ ).

Despite this reassuring similarity in values reported here and by Luo *et al* (2009), the fit between the simulated indentation curves using the optimal orthotropic elastic parameters and measured curves is not exact as shown in Figure 2.8. This is most likely because only geometric nonlinearity was taken into account in the FE models. Improvements could result if material intrinsic nonlinearities are also considered. The measured response curves for the three animals differ from each other because of interspecimen differences in local material properties, thickness and local surface geometry (Hesabgar *et al*, 2010).

Estimates of  $E_x$ ,  $E_y$ , and  $G_{xy}$  made using the indentation-based and pressurization-based approaches do not vary with modeling assumptions made about the thickness and Young's modulus of the pars flaccida, ligament or manubrium. The pars flaccida is much more compliant than the pars tensa and represents only a small fraction of the total eardrum surface area in comparison to the pars tensa. It is observed that its mechanical behavior is not tightly coupled to that of the pars tensa (Funnell and Laszlo, 1978). Hence, it is unlikely that changes in the properties of the model pars flaccida would affect estimates of  $E_x$ ,  $E_y$ , and  $G_{xy}$  for the pars tensa as long as the pars flaccida is indeed constrained to be more compliant than the pars tensa in the FE models. The ligament and manubrium are essentially rigid in comparison to the pars tensa, and variations in their properties would not be expected to affect  $E_x$ ,  $E_y$ , and  $G_{xy}$  as long as the model ligament and manubrium remain rigid despite these variations.

$E_x$  and  $E_y$  do vary significantly with the thickness of the model pars tensa; however,  $G_{xy}$  does not. As the thickness increases, estimates of  $E_x$  and  $E_y$  must decrease in order to maintain the same overall structural stiffness. Hesabgar *et al* (2010) also observed that their estimate of the Young's modulus in their isotropic model of the pars tensa decreases as the thickness of the model pars tensa increases. Micro-CT as used here cannot resolve the variations in pars tensa thickness over its surface. Confocal microscopy is indeed suitable (Kuypers *et al*, 2005a, 2005b, 2006), but has not been applied to rats. This work highlights the need for measurement of thickness variations in this important species for hearing research.

## 2.5. Conclusion

Two techniques were developed to estimate the orthotropic elastic parameters of the rat eardrum, an indentation-based technique and a pressurization-based technique. Tests on synthetic data indicate that the pressurization-based technique is more robust to simulated noise than the indentation-based technique. The former attains an accuracy in excess of 90% for an SNR of 2 or greater in the measurements. The indentation-based technique requires an SNR of 200 or greater for the same level of accuracy. Although in general the simplex optimization method requires initialization values that are not very different from the correct moduli values, both the indentation and pressurization techniques as described here are robust to a wide range of initialization values. Estimates of  $E_x = 23.39 \pm 1.55$  MPa,  $E_y = 58.67 \pm 4.16$  MPa, and  $G_{xy} = 35.56 \pm 3.29$  MPa were obtained for rat eardrums using the indentation-based technique for which prior data were available. These estimates are insensitive to all other modeling parameters except for pars tensa thickness.

## 2.4. References

- Aernouts, J., Soons, J.A., Dirckx, J.J., 2010. Quantification of tympanic membrane elasticity parameters from in situ point indentation measurements: Validation and preliminary study. *Hear. Res.*, 263(1-2), 177-182.
- Akache, F., Funnell, W.R., Daniel, S.J., 2007. An experimental study of tympanic membrane and manubrium vibrations in rats, *Audiol.Neurotol.* 12 49-58.
- Békésy, G.v., 1960. *Experiments in Hearing*, McGraw-Hill, Toronto, ON.
- Cheng, T., Dai, C., Gan, R.Z., 2007. Viscoelastic properties of human tympanic membrane. *Ann. Biomed. Eng.*, 35 (2) 305-314.
- Courtis, R.P., 2007. *Constrained prostate ultrasound elastography using mutual information*, Faculty of Graduate Studies, University of Western Ontario, London, Ont.
- Daniel, S.J., Funnell, W.R.J., Zeitouni, A.G., Schloss, M.D., Rappaport, J., 2001. Clinical applications of a finite-element model of the human middle ear. *J. Otolaryngol.* 30 (6), 340-346.
- Daphalapurkar, N.P., Dai, C., Gan, R.Z., Lu, H., 2009. Characterization of the linearly viscoelastic behavior of human tympanic membrane by nanoindentation. *J. Mech. Behav. Biomed. Mater.*, 2 (1) 82-92.
- Decraemer, W.F., Dircks, J.J.J., Funnell, W.R.J., 1991. Shape and derived geometrical parameters of the adult, human tympanic membrane measured with a phase-shift moiré interferometer., *Hear.Res.* (51) 107-121.
- Decraemer, W.F., Maes, M.A., Vanhuyse, V.J., 1980. An elastic stress-strain relation for soft biological tissues based on a structural model. *J. Biomech.*, 13 (6) 463-468.
- Dirckx, J.J., Decraemer, W.F., 1997. Coating techniques in optical interferometric metrology, *Appl.Opt.* 36, 2776-2782.
- Ethier, C.R., and Simmons, C.A., 2007. *Introductory Biomechanics from Cells to Organisms*, Cambridge University Press, Cambridge, UK.

- Fay, J.P., Puria, S., Steele, C.R., 2006. The discordant eardrum, Proc.Natl.Acad.Sci.U.S.A. 103, 19743-19748.
- Funnell, W.R.J., Khanna, S.M., Decraemer, W.F., 1992. On the degree of rigidity of the manubrium in a finite-element model of the cat eardrum. J. Acoust. Soc. Am. 91 (4), 2082–2090.
- Funnell, W.R.J., Laszlo, C.A., 1978. Modeling of the cat eardrum as a thin shell using the finite- element method. J. Acoust. Soc. Am., 63 (5) 1461-1467
- Funnell, W.R.J., Laszlo C.A., 1982. A critical review of experimental observations on ear-drum structure and function. ORL., 44(4) 181-205.
- Gaihede, M., Liao, D., Gregersen, H., 2007. In vivo areal modulus of elasticity estimation of the human tympanic membrane system: modelling of middle ear mechanical function in normal young and aged ears. Phys. Med. Biol., 52 (3) 803-814.
- Gan, R.Z., Cheng, T., Dai, C., Yang, F., Wood, M.W., 2009. Finite element modeling of sound transmission with perforations of tympanic membrane, J.Acoust.Soc.Am. 126, 243-253.
- Gan, R.Z., Sun, Q., Feng, B., Wood, M.W., 2006. Acoustic-structural coupled finite element analysis for sound transmission in human ear--pressure distributions, Med.Eng.Phys. 28, 395-404.
- Gentil, F., Parente, M., Martins, P., Garbe, C., Jorge, R.N., Ferreira, A., et al. 2011. The influence of the mechanical behavior of the middle ear ligaments: A finite element analysis, Proc.Inst.Mech.Eng.Part H J.Eng.Med. 225, 68-76.
- Hesabgar, S.M., Marshall, H., Agrawal, S. K., Samani, A., Ladak, H.M., 2010. Measuring the quasi-static Young's modulus of the eardrum using an indentation technique. Hear. Res., 263(1-2), 168-176.
- Huang, G., Daphalapurkar, N.P., Gan, R.Z., Lu, H., 2008. A Method for measuring linearly viscoelastic properties of human tympanic membrane using nanoindentation. J. Biomech. Eng., 130 (1) 014501.

- Jahromi, S.N.G., 2009. Estimation of the quasi-static Young's modulus of the rat eardrum using a pressurization method, School of Graduate and Postdoctoral Studies, University of Western Ontario, London, Ont.
- Kirikae, I., 1960. The Structure and Function of the Middle Ear. University of Tokyo Press, Tokyo.
- Knupp, P., and Steinberg, S., 1993. Fundamentals of Grid Generation, CRC Press, Boca Raton, FL.
- Kuypers, L.C., Decraemer, W.F., Dirckx, J.J., Timmermans, J.P., 2005a. Thickness distribution of fresh eardrums of cat obtained with confocal microscopy, *J.Assoc.Res.Otolaryngol.* 6, 223-233.
- Kuypers, L.C., Dirckx, J.J., Decraemer, W.F., Timmermans, J.P., 2005b. Thickness of the gerbil tympanic membrane measured with confocal microscopy, *Hear.Res.* 209, 42-52.
- Kuypers, L.C., Decraemer, W.F., Dirckx, J.J., 2006. Thickness distribution of fresh and preserved human eardrums measured with confocal microscopy. *Otology & Neurotology* 27, 256–264.
- Ladak, H.M., Decraemer, W.F., Dirckx, J.J., Funnell, W.R., 2004. Response of the cat eardrum to static pressures: mobile versus immobile malleus, *J.Acoust.Soc.Am.* 116, 3008-3021.
- Lagarias, J.C., Reeds, J.A., Wright, M.H., and Wright, P.E., 1998. Convergence Properties of the Nelder-Mead Simplex Method in Low Dimensions. *SIAM J. Optim.*, vol. 9 Number 1, pp. 112-147.
- Lim, D.J., 1968. Tympanic membrane. Electron microscopic observation. I: pars tensa. *Acta Oto-laryngologica* 66 (3), 181–198.
- Lim, D.J., 1970. Human tympanic membrane. An ultrastructural observation. *Acta Oto-laryngologica* 70 (3), 176–186.
- Liu Hou-guang, Na, T., Rao Zhu-shi. 2009. Numerical Simulation of Human Middle Ear Based on Finite-Element Method, *Journal of System Simulation.* 21, 7899-901.

Luo, H., Dai, C., Gan, R.Z., Lu, H., 2009. Measurement of young's modulus of human tympanic membrane at high strain rates. *Journal of Biomechanical Engineering* 131, 064501-1.8.

Mow, V.C., Huiskes, R., 2005. *Basic Orthopaedic Biomechanics and Mechano- Biology*, third ed. Lippincott Williams and Wilkins, PA.

O'Hagan, J.J., Samani, A., 2008. Measurement of the hyperelastic properties of tissue slices with tumour inclusion. *Phys. Med. Biol.* 53 (24), 7087–7106.

Samani, A., Bishop, J., Luginbuhl, C., Plewes, D.B., 2003. Measuring the elastic modulus of ex vivo small tissue samples. *Phys. Med. Biol.* 48 (14), 2183–2198.

Takeda, M., and Mutoh, K., 1983. Fourier transform profilometry for the automatic measurement of 3D object shapes," *Appl. Opt.*, vol. 22, Issue 24, pp. 3977-3982.

Tuck-Lee, J.P., Pinsky, P.M., Steele, C.R., Puria, S., 2008. Finite element modeling of acousto-mechanical coupling in the cat middle ear. *J. Acoust. Soc. Am.*, 124 (1) 348-362.

Volandri, G., Di Puccio, F., Forte, P., Carmignani, C., 2011. Biomechanics of the tympanic membrane, *J.Biomech.* 44, 1219-1236.

Wang, J., Zhao, F., Li, Y., Han, D., Gong, S., Zhao, S., et al. 2011. Effect of anterior tympanomeatal angle blunting on the middle ear transfer function using a finite element ear model, *Med.Eng.Phys.*

Yao Wen-juan, Wu, L., Fu Li-Jie, Huang Xin-sheng. 2009. Numerical simulation and transmitting vibration analysis for middle-ear structure, *Journal of System Simulation.* 21, 651-4.

Zhu, Y., Chen, L., Zhang, T., Dai, P., Xie, Y., Yang, L., et al. 2010. Finite element modeling for a human tympanic membrane with sections of polymer-embedded temporal bone, *Zhendong yu Chongji/Journal of Vibration and Shock.* 29, 117-121.



## Chapter 3

### 3.1. Contributions

The main contribution of this work is to the development and evaluation of two *in situ* techniques for estimating the orthotropic elastic properties of the pars tensa of the eardrum. Specifically, the indentation-based technique developed by Hesabgar *et al* (2010) and the pressurization-based technique developed by Jahromi (2010) were extended by incorporating a linearly elastic orthotropic model of the pars tensa into the optimization framework. In the previous studies, the authors had used a linear elastic isotropic model of the pars tensa. This modification changed the estimation task from a univariate optimization problem (i.e., only the Young's modulus,  $E$ , was required) to a multivariate problem requiring the estimation of  $E_x$ ,  $E_y$  and  $G_{xy}$ . Therefore, the univariate optimization methods used by the previous authors could not be used here. Instead, a variant of the Nelder-Mead simplex method (Lagarias *et al*, 1998) was used.

Another contribution of this work is in the application of the indentation-based technique to estimating  $E_x$ ,  $E_y$  and  $G_{xy}$  for the rat eardrum. These estimates provide important input parameters for future modeling efforts that are being undertaken by others for this important experimental animal. The effects on these estimates of varying modeling parameters that are not well known was also quantified, and revealed that  $E_x$  and  $E_y$  are particularly sensitive to the thickness of the pars tensa model.

### 3.2. Future Considerations

Based on experience acquired during this work, several refinements are suggested. These include modifications to the cost functions used, comparison of numerical optimization algorithms used to minimize these cost functions and refining the quality of the FE models used for optimization. The cost function for the indentation-based method and that for the pressurization-based method both have a single global minimum within the upper and lower bounds set on the search space. However, this minimum is relatively broad and shallow, and the simplex method used crawls to the final optimum. It would be possible to speed up convergence by appropriately redesigning the cost functions to have a narrow, steep minimum by defining the cost function to be a weighted sum of the indentation cost function and the pressurization cost function. The disadvantage of this would be that both types of response data (force-displacement curves and pressurized eardrum shapes) would need to be acquired for a given estimation task. Currently, only one or the other type of data needs to be acquired.

A variant of the Nelder-Mead simplex algorithm (Lagarias *et al*, 1998) was used to find the global minimum. This algorithm does not require the computation of the derivatives of the cost function with respect to each independent variable. Although this makes the simplex algorithm less prone to noise in the cost function evaluation that may come about because of noisy experimental data, the algorithm is slow. Given that experimentally acquired indentation data and pressurized shape data have high SNR values, one might opt for faster gradient-based optimization methods.

Since the publication of first journal paper describing the use of FE modeling to simulate the response of the eardrum (Funnell and Laszlo, 1978), significant effort has gone towards refining models of the eardrum. Based on the present study, the most important modeling parameter that affects estimates of  $E_x$  and  $E_y$  is the thickness of the pars tensa. Although confocal microscopy has been used to measure the thickness of the eardrum in other species (Kuypers *et al*, 2005a, 2005b, 2006), it has not been applied to the rat eardrum. Such measurements need to be made for the rat since it is an important animal in hearing biomechanics research. Confocal microscopy provides point measurements of eardrum thickness, and it is time consuming to apply it to measure variations in thickness across the surface of the eardrum. Micro-CT has also been applied to measure the thickness of the human eardrum (Puria *et al*, 2006). This results in a full-field thickness map. However, to obtain reasonable SNR values at the required resolutions, long scan times are required and special care needs to be taken to mitigate drying of the eardrum and subsequent shrinkage, especially for the rat eardrum which is thinner than the human eardrum.

Modeling the behavior of the eardrum to large loads as done in this work is important in understanding its response to barotrauma, surgery and diagnostics (Ladak *et al*, 2006). Although geometric nonlinearity accounts for some of the nonlinearity seen in force-displacement curves, intrinsic nonlinear material models are required to improve the fit between simulation results and experimental data.

Ultimately, FE models of the human eardrum are required, not just of the rat eardrum. Hence, once the techniques are refined on synthetic data and animal data, they need to be applied to fresh human tissue, which is generally difficult to acquire. *In vivo*

testing may be possible in humans by developing an indenter that could be introduced through the ear canal. Moreover, *in vivo* shape measurements utilizing endoscopic moiré profilometers may become possible in the future based on the preliminary designs of nez-Celerio *et al* (2004).

Johnson, P. A. (1988). *Estimation of the ear-canal cross-section of the ear-canal*. Ph.D. Thesis, University of Western Australia, Perth, Australia.

Johnson, P. A., Brown, J. C., Wilson, J. H., and Wright, B. C. (1988). *Computerized measurement of the middle-ear volume from an ear-canal cross-section*. *JAMA*, 260, 1111-1115.

Johnson, P. A. (1991). *Estimation of the ear-canal cross-section of the ear-canal*. Ph.D. Thesis, University of Western Australia, Perth, Australia.

Johnson, P. A., Brown, J. C., Wilson, J. H., and Wright, B. C. (1988). *Computerized measurement of the middle-ear volume from an ear-canal cross-section*. *JAMA*, 260, 1111-1115.

Johnson, P. A., Brown, J. C., Wilson, J. H., and Wright, B. C. (1988). *Computerized measurement of the middle-ear volume from an ear-canal cross-section*. *JAMA*, 260, 1111-1115.

Johnson, P. A., Brown, J. C., Wilson, J. H., and Wright, B. C. (1988). *Computerized measurement of the middle-ear volume from an ear-canal cross-section*. *JAMA*, 260, 1111-1115.

Johnson, P. A., Brown, J. C., Wilson, J. H., and Wright, B. C. (1988). *Computerized measurement of the middle-ear volume from an ear-canal cross-section*. *JAMA*, 260, 1111-1115.

Johnson, P. A., Brown, J. C., Wilson, J. H., and Wright, B. C. (1988). *Computerized measurement of the middle-ear volume from an ear-canal cross-section*. *JAMA*, 260, 1111-1115.

Johnson, P. A., Brown, J. C., Wilson, J. H., and Wright, B. C. (1988). *Computerized measurement of the middle-ear volume from an ear-canal cross-section*. *JAMA*, 260, 1111-1115.

### 3.2. Reference

- Hesabgar, S.M., Marshall, H., Agrawal, S. K., Samani, A., Ladak, H.M., 2010. Measuring the quasi-static Young's modulus of the eardrum using an indentation technique. *Hear. Res.*, 263(1-2), 168-176.
- Jahromi, S.N.G., 2009. Estimation of the quasi-static Young's modulus of the rat eardrum using a pressurization method, School of Graduate and Postdoctoral Studies, University of Western Ontario, London, Ont.
- Lagarias, J.C., Reeds, J.A., Wright, M.H., and Wright, P.E., 1998. Convergence Properties of the Nelder-Mead Simplex Method in Low Dimensions. *SIAM J. Optim.*, vol. 9 Number 1, pp. 112-147.
- Press, W.H., Teukolsky, S.A., 1992. Numerical recipes, *Comput.Phys.* 6, 670-670.
- Funnell, W.R.J., Laszlo, C.A., 1978. Modeling of the cat eardrum as a thin shell using the finite- element method. *J. Acoust. Soc. Am.*, 63 (5) 1461-1467.
- Kuypers, L.C., Decraemer, W.F., Dirckx, J.J., Timmermans, J.P., 2005a. Thickness distribution of fresh eardrums of cat obtained with confocal microscopy, *J.Assoc.Res.Otolaryngol.* 6, 223-233.
- Kuypers, L.C., Dirckx, J.J., Decraemer, W.F., Timmermans, J.P., 2005b. Thickness of the gerbil tympanic membrane measured with confocal microscopy, *Hear.Res.* 209, 42-52.
- Kuypers, L.C., Decraemer, W.F., Dirckx, J.J., 2006. Thickness distribution of fresh and preserved human eardrums measured with confocal microscopy. *Otology & Neurotology* 27, 256-264.
- Puria, S., Sim, J.H., Tuck-Lee, J., Steele, C.R. (2006) "Middle ear morphometry from cadaveric temporal bone microCT imaging" In *Proceedings of the 4th International Symposium Middle Ear Mechanincs in Research and Otology*. Edited by A. Eiber and A. Huber. World Scientific.
- HM Ladak, WR Funnell, WF Decraemer, JJ Dirckx. A geometrically nonlinear finite-element model of the cat eardrum, *J.Acoust.Soc.Am.* 119 (2006) 2859-2868.

RA Martı nez-Celorio, JJJ Dirckx, L Martı -Lopez, FG Pena-Lecona. Out-of-plane displacement measurement by means of endoscopic moiré interferometry, Review of Scientific Instruments. 75 (2004) 492-496.

ARTICLE IN PRESS

REVISED MANUSCRIPT

ACCEPTED MANUSCRIPT

ACCEPTED MANUSCRIPT

Final review by the Societat Espanyola de Física i Matemàtiques (SEFIM) for the Department of Physics and Mathematics of the Universitat de València. The authors thank the Universitat de València for the financial support of this work. The authors also thank the Universitat de València for the financial support of this work. The authors also thank the Universitat de València for the financial support of this work.